(2)

IDA PAPER P-2083

IDA GAMMA-RAY LASER ANNUAL SUMMARY REPORT (1987)

INVESTIGATION OF THE FEASIBILITY OF DEVELOPING A LASER USING NUCLEAR TRANSITIONS

Bohdan Balko
Leslie Cohen
David A. Sparrow
Jeffrey F. Nicoll

December 1988

Prepared for
Strategic Defense Initiative Organization
Innovative Science and Technology Office
Dwight Duston, Acting Director

IDA
INSTITUTE FOR DEFENSE ANALYSES
1801 N. Beauregard Street, Alexandria, Virginia 22311-1772

IDA Log No. HQ 87-33002

DEFINITIONS

IDA publishes the following documents to report the results of its work.

Reports

Reports are the most authoritative and most carefully considered products IDA publishes. They normally embody results of major projects which (a) have a direct bearing on decisions affecting major programs, or (b) address issues of significant concern to the Executive Branch, the Congress and/or the public, or (c) address issues that have significant economic implications. IDA Reports are reviewed by outside panels of experts to ensure their high quality and relevance to the problems studied, and they are released by the President of IDA.

Papers

Papers normally address relatively restricted technical or policy issues. They communicate the results of special analyses, interim reports or phases of a task, ad hoc or quick reaction work. Papers are reviewed to ensure that they meet standards similar to those expected of refereed papers in professional journals.

Memorandum Reports

IDA Memorandum Reports are used for the convenience of the sponsors or the analysts to record substantive work done in quick reaction studies and major interactive technical support activities; to make available preliminary and tentative results of analyses or of working group and panel activities; to forward information that is essentially unanalyzed and unevaluated; or to make a record of conferences, meetings, or briefings, or of data developed in the course of an investigation. Review of Memorandum Reports is suited to their content and intended use.

The results of IDA work are also conveyed by briefings and informal memoranda to sponsors and others designated by the sponsors, when appropriate.

The work reported in this document was conducted under contract MDA 903 84 C 0031 for the Department of Defense. The publication of this IDA document does not indicate endorsement by the Department of Defense, nor should the contents be construed as reflecting the official position of that agency.

This paper has been reviewed by IDA to assure that it meets high standards of thoroughness, objectivity, and sound analytical methodology and that the conclusions stem from the methodology.

Approved for public release: distribution unlimited.

UNCLASSIFIED
SECURITY CLASSIFICATION OF THIS PAGE

REPORT DOCUMENTATION PAGE

1a. REPORT SECURITY CLASSIFICATION UNCLASSIFIED	1b. RESTRICTIVE MARKINGS
2a. SECURITY CLASSIFICATION AUTHORITY NA	3. DISTRIBUTION/AVAILABILITY OF REPORT Approved for public release; distribution unlimited.
2b. DECLASSIFICATION/DOWNGRADING SCHEDULE NA	
4. PERFORMING ORGANIZATION REPORT NUMBER(S) IDA Paper P-2083	5. MONITORING ORGANIZATION REPORT NUMBER(S)
6a. NAME OF PERFORMING ORGANIZATION Institute for Defense Analyses 6b. OFFICE SYMBOL (If applicable)	7a. NAME OF MONITORING ORGANIZATION DoD-IDA Management Office, OUSDRE
6c. ADDRESS (City, State, and Zip Code) 1801 N. Beauregard Street Alexandria, VA 22311	7b. ADDRESS (CITY, STATE, AND ZIP CODE) 1801 N. Beauregard Street Alexandria, VA 22311
8a. NAME OF FUNDING/SPONSORING ORGANIZATION Strategic Defense Initiative Organization 8b. OFFICE SYMBOL (If applicable)	9. PROCUREMENT INSTRUMENT IDENTIFICATION NUMBER MDA 903 84 C 0031
8c. ADDRESS (City, State, and Zip Code) The Pentagon Washington, DC 20301-7100	10. SOURCE OF FUNDING NUMBERS PROGRAM ELEMENT / PROJECT NO. / TASK NO. T-R2-316 / WORK UNIT ACCESSION NO.

11. TITLE (Include Security Classification) IDA Gamma-Ray Laser Annual Summary Report (1987):
Investigation of the Feasibility of Developing a Laser Using Nuclear Transitions

12. PERSONAL AUTHOR(S).
Bohdan Balko, Leslie Cohen, David A. Sparrow, Jeffrey F. Nicoll

13. TYPE OF REPORT	13b. TIME COVERED	14. DATE OF REPORT (Year, Month, Day)	15. PAGE COUNT
Final	FROM 10/86 TO 9/87	December 1988	87

16. SUPPLEMENTARY NOTATION

17. COSATI CODES			18. SUBJECT TERMS (Continue on reverse if necessary and identify by block number)
FIELD	GROUP	SUB-GROUP	Nuclear Laser, Gamma-ray laser, Graser, Superradiance, Mössbauer effect, Borrmann effect, Nuclear Isomers, Nuclear magnetic resonance, line-narrowing, Nuclear data, Nuclear structure, inhomogenous broadening, energy deposition, temperature rise during pumping

19. ABSTRACT (Continue on reverse if necessary and identify by block number)

This report summarizes the IDA research effort in FY 1987 in investigating the feasibility of developing a γ-ray laser.

20. DISTRIBUTION/AVAILABILITY OF ABSTRACT	21. ABSTRACT SECURITY CLASSIFICATION	
☐ UNCLASSIFIED/UNLIMITED ☒ SAME AS RPT. ☐ DTIC USERS	UNCLASSIFIED	
22a. NAME OF RESPONSIBLE INDIVIDUAL Bohdan Balko	22b. TELEPHONE (Include Area Code) (703) 578-2991	22c. OFFICE SYMBOL

DD FORM 1473, 84 MAR 83 APR edition may be used until exhausted. All other editions are obsolete

SECURITY CLASSIFICATION OF THIS PAGE
UNCLASSIFIED

IDA PAPER P-2083

IDA GAMMA-RAY LASER ANNUAL SUMMARY REPORT (1987)

INVESTIGATION OF THE FEASIBILITY OF DEVELOPING A LASER USING NUCLEAR TRANSITIONS

Bohdan Balko
Leslie Cohen
David A. Sparrow
Jeffrey F. Nicoll

December 1988

INSTITUTE FOR DEFENSE ANALYSES

Contract MDA 903 84 C 0031
Task T-R2-316

PREFACE

In January 1985, Dr. James A. Ionson, then Director of the Science and Technology Directorate of the Strategic Defense Initiative Organization (SDIO) asked members of the IDA research staff to investigate the feasibility of developing a gamma-ray laser. The staff determined what work had been done, who was currently working in the field, and what work should be encouraged or supported. Then a workshop was convened for research workers directly involved both in gamma-ray laser work and in ancillary fields such as nuclear structure, radiation propagation in crystals, Mössbauer effect, and optical lasers. Next, an in-house study was undertaken to clarify critical issues concerning the various pumping schemes proposed at the workshop as well as systems questions about the gamma-ray laser as a working device.

The proceedings of the workshop were published in the form of a report to the Innovative Science and Technology Office (IST) of the SDIO. The work completed in 1985 is presented in IDA Paper P-2021, "IDA Gamma-Ray Laser Annual Summary Report (1985): Investigation of the Feasibility of Developing a Laser Using Nuclear Transitions" (Ref. 1).

In 1986, the in-house work focused on extending the data base, the nature of superradiance in the gamma-ray laser context, and a detailed investigation of the upconversion pumping scheme. A discussion of nuclear systematics, investigations of electron-nuclear-driven pumping, and lifetime measurements rounded out that study. The results of the FY 1986 effort are presented in IDA paper, P-2004 (Ref. 2).

The development of a gamma-ray laser is viewed as a high-risk/high-payoff undertaking. IDA's involvement focuses on minimizing the risk and on striving to redirect the effort when proposed schemes are shown not to be feasible.

In 1987, the IDA research staff looked at the state of the art and assessed the situation in gamma-ray laser work (described in Chapter I). Focus was on two areas of research interest critical to three concepts for developing a gamma-ray laser. In Chapter II the heating effects associated with upconversion techniques are discussed. Although the

work concentrated on the direct upconversion of nuclei with electromagnetic radiation, the results of the studies also apply to upconversion through the mechanism of electron-nuclear coupling. In the second study (Chapter III), the sources of inhomogeneous broadening which destroy the Mössbauer effect are investigated and the techniques available for restoring the resonance (destroying the effect of inhomogeneous broadening) by external or internal fields are considered. An old concept for doing this is reviewed and two new approaches are introduced.

This report does not have an overall introduction. Each chapter is an independent study containing its own introduction.

ABSTRACT

This report summarizes the IDA research effort in FY 1987 in investigating the feasibility of developing a γ-ray laser.

CONTENTS

FIGURES

TABLES

SUMMARY

This report describes the 1987 research effort by members of the IDA staff in the field of gamma-ray lasers. The work is part of a continuing task in support of the Innovative Science and Technology Office (IST) of the Strategic Defense Initiative Organization (SDIO). The development of a gamma-ray laser is a high-risk science and technology undertaking. IDA involvement has focused in large measure on minimizing the risk and attempting to redirect the program as quickly as possible when proposed schemes prove infeasible. The report is presented in three independent chapters.

Chapter I is a tutorial overview of the subject of gamma-ray lasers. It presents a review of the problems specific to nuclear transitions that make the task of building a nuclear laser more difficult than building conventional lasers. A unique two-step approach is taken, showing first that a gas laser is possible, in principle, then considering a crystalline laser. Then, assuming that a gamma-ray laser is feasible, major problem areas requiring study are pointed out. These include establishment of laser-specific nuclear data bases, production of samples of the right nuclear species, fabrication of the required crystals, and detailed studies of radiation transport and coherent emission. The three major lasing schemes that have been proposed are discussed, along with the specific problems that will have to be overcome in each case.

Chapter II takes a critical look at the heating effects associated with upconversion techniques. Sample calculations for x-ray upconversion in very thin wires of ^{57}Fe lead to phase changes from heating which destroy the lattice and therefore the Mössbauer effect. Preliminary calculations indicate that conductive cooling of the wire is not a viable option. It is therefore suggested that other pumping schemes receive greater attention.

Chapter III reexamines the long-lifetime concept of developing a gamma-ray laser. The major difficulty with this scheme is inhomogeneous broadening. The problem is approached from two extremes. In one, the broadening is, in principle, removed through the use of RF pulses which undo the effects of the dipole-dipole interactions in the crystal. In the other approach, the level is homogeneously broadened through level mixing

spectroscopy techniques or through relaxation effects. The enhanced broadening increases the overlap of transitions and may produce an increase in the nuclear resonance. Further work has to be done to determine the effect on the nuclear cooperative emission or superradiance.

I. ASPECTS OF THE CURRENT STATUS OF THE GRASER

A. INTRODUCTION

At the core of every atom is a small entity, the nucleus. The radius of the nucleus is of the order of a few femtometers, i.e., it is about five orders of magnitude smaller than the atom. It is a system of many particles and is amenable to a quantum-mechanical description. The particles give rise to charge distributions and currents which are the sources of the electromagnetic radiation that we are interested in. This radiation, both in its multipole character and in its interactions with matter, is quite different from the longer wavelength radiation emitted during changes in the electronic structure of the atom. As in the case of the atom, the nucleus is characterized by a complex eigenvalue spectrum. Our goal is to study the feasibility of a laser based on an electromagnetic transition between two of the levels in a particularly suitable nucleus.

Figure 1 shows a modification of an historical plot by D. J. Nagle. (Ref. 3) The graph shows the peak energy, as a function of time, of new sources of coherent radiation. The two highest points (represented by squares) and a shaded horizontal band have been added. The points represent two reported x-ray lasers and the band shows the approximate region of interest for the prospective graser, roughly from less than 100 eV to more than 100 keV. A major reason for the interest in nuclear lasers is the availability of a region of higher photon energy and the concomitant possibilities of higher densities of energy storage and more intense and more penetrating beams. To see the contrast between nuclear and atomic structure, it is worth observing the level structure of two typical nuclei, one light and one heavy. Figure 2 is an energy level diagram of ^{11}C. The contrast to an atomic case is immediately obvious as excitation energies are of the order of MeV, not eV. The lower levels decay only by photon emission, but the higher states have other modes. For example, a state above 7.55 MeV can decay by the emission of an alpha particle, leaving a ^{7}Be nucleus. Conversely, these states can be formed by bombarding a ^{7}Be target with sufficiently energetic alpha particles. Figure 3 shows the energy level diagram of a very

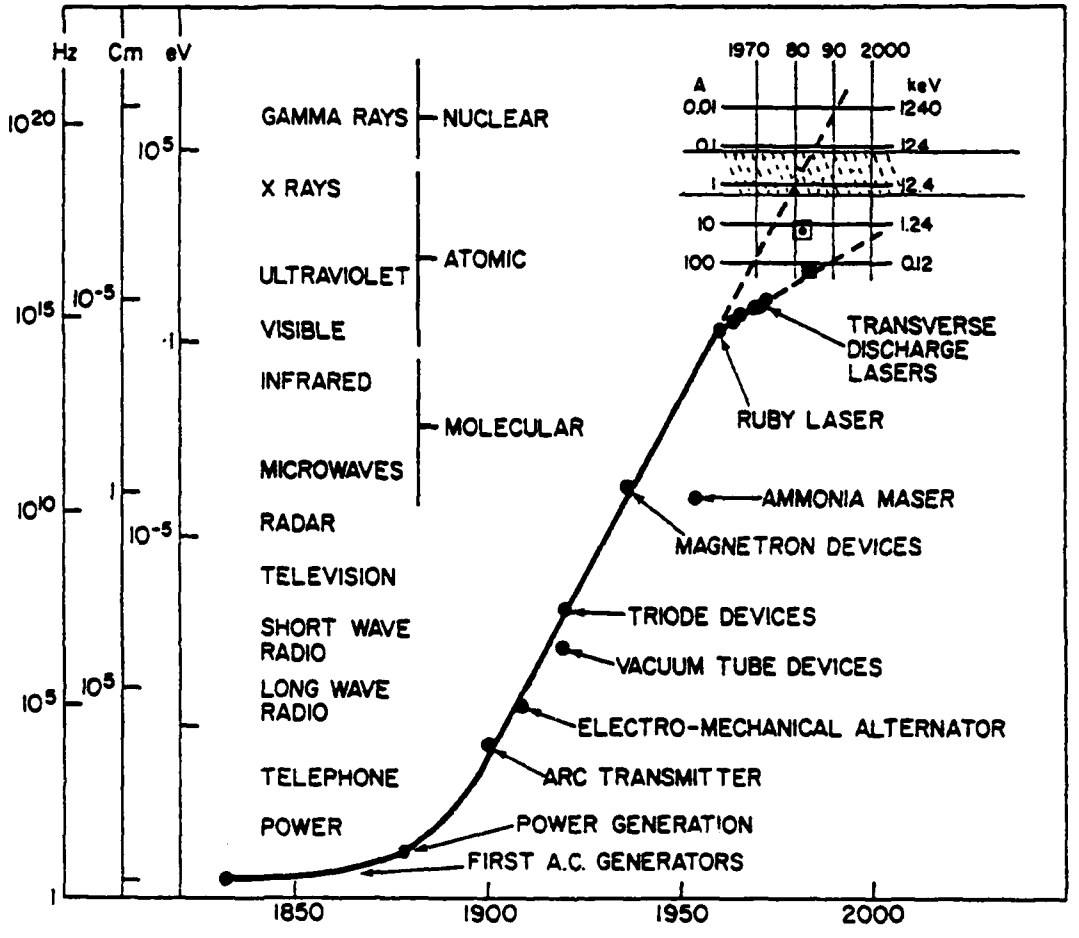

Figure 1. Nagle's historical growth curve for the generation of coherent electrical and electromagnetic waves. It should be noted that the ranges marked nuclear, atomic, molecular are rough. They merely indicate the sources of the radiation. In fact, the ranges of gamma-rays and x-rays strongly overlap in the KeV regime.

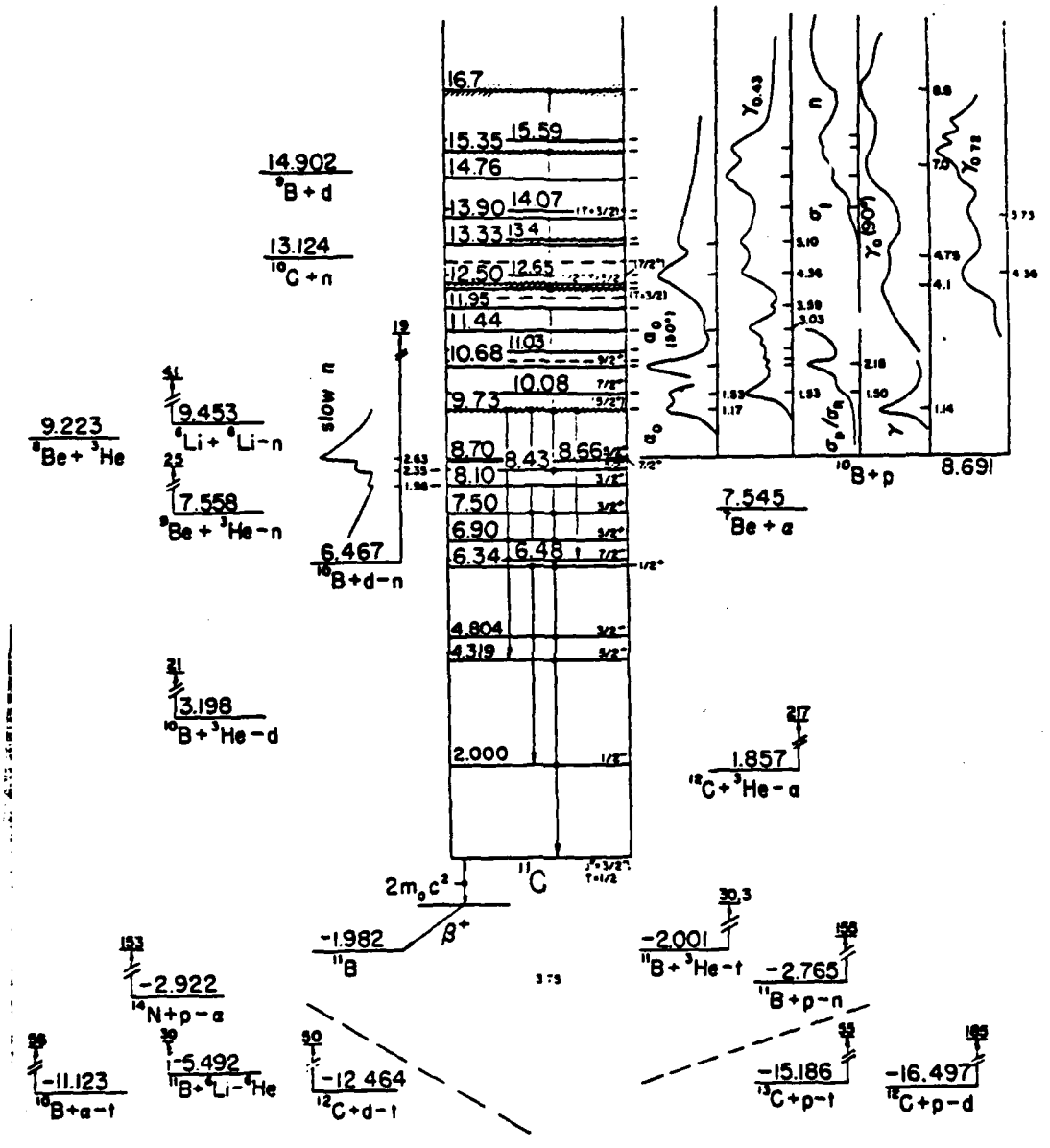

Figure 2. The level spectrum of ^{11}C. Energy of excitation is given in MeV.

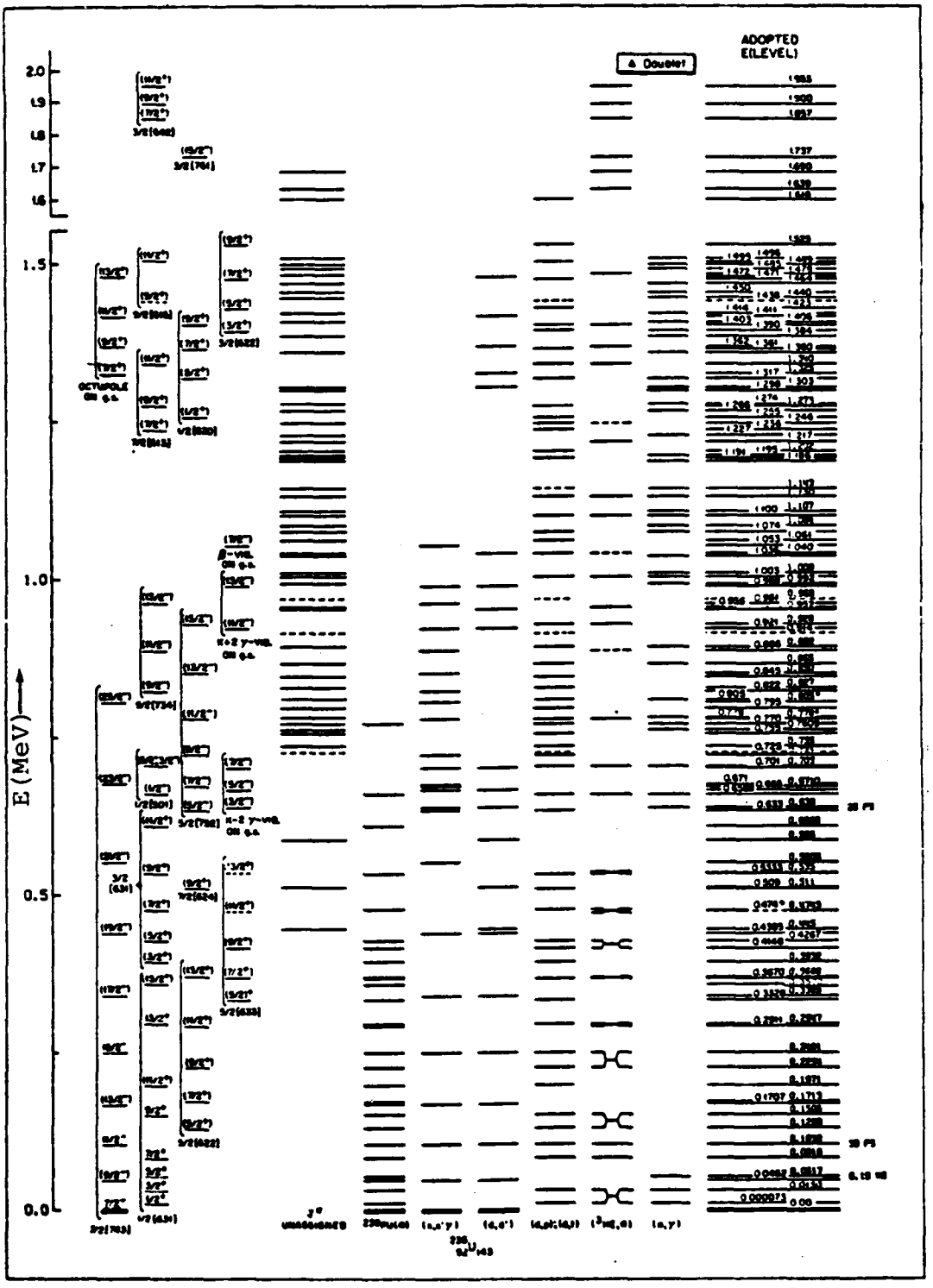

Figure 3. The level spectrum of 235U is shown for an excitation range of 2 MeV. The location of the lowest state at 73 eV is exaggerated.

heavy nucleus, ^{235}U. In the 2 MeV of excitation for which only one level appeared in the carbon nucleus (Fig. 2), there are now about 100 levels (Fig. 3); and the first excited state has an energy of only 73 eV, the lowest known first excited state of a nucleus. This level plays a role in one of the schemes. At the current level of nuclear theory, these spectra cannot be predicted with any precision.

Again, our goal is to study the gamma-ray laser--a conceptual device based either on stimulation or superradiance. It is based on a transition between two nuclear levels. As a first guess, the nuclei will be embedded in a crystal or gas having an acicular shape.

B. MULTIPOLE RADIATION

The sketch in Fig. 4 represents radiation of frequency ω that is emitted when a transition occurs between the two levels.

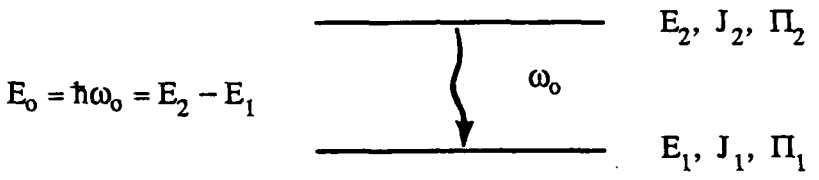

Figure 4. The two-level system.

The power that is radiated can be expressed as a series of two terms:

$$P(\omega) = \sum_l \left[P_{l,m}(\omega,E) + P_{l,m}(\omega,M)\right] \qquad (1)$$

$$= \sum_l \frac{2(l+1)}{l\,[(2l+1)!!]^2}\, c\left[\frac{\omega}{c}\right]^{2(l+1)} \left[\frac{1}{\varepsilon_o}\left|Q_{l,m}\right|^2 + \mu_o \left|M_{l,m}\right|^2\right] \text{ Watts.}$$

The first terms, the electric multipoles, are due to the charge distributions in the nucleus:

$$Q_{l,m} = \int r^l\, Y^*_{l,m}(\theta,\phi)\, P(r)\, d\tau \rightarrow e \sum_{k=1}^{Z} \int r_k^l\, Y^*_{l,m}(\theta_k,\phi_k)\, \psi_2^*\psi_1^*\, d\tau\,. \qquad (2)$$

The second set of terms, the magnetic multipoles, are due to currents and are given by:

$$M_{l,m} = \int r^l Y^*_{l,m}(\theta,\phi) \frac{\vec{\nabla}(\vec{r} \times \vec{j})}{l+1} d\tau \rightarrow \frac{1}{l+1} \frac{eh}{M_p} \sum_{k=1}^{Z} \int r_k^l Y^*_{l,m}(\theta_k,\phi_k) \vec{\nabla} (\psi_2^* \vec{L}_k \psi_1) d\tau,$$

where

$$L_k = -i\vec{r}_k \times \vec{\nabla}_k . \qquad (3)$$

Each term gives the power radiated by that particular electric or magnetic multipole, and the corresponding decay constants are given by

$$\lambda_{l,m}(E) = \frac{P_{l,m}(E)}{\hbar\omega}$$

and

$$\lambda_{l,m}(M) = \frac{P_{l,m}(M)}{\hbar\omega} . \qquad (4)$$

The corresponding lifetimes are given by

$$\tau_{l,m} = \frac{1}{\lambda_{l,m}} . \qquad (5)$$

In general, the number of terms in the expansion are limited to just a few by selection rules on angular momentum and parity. These are:

Angular Momentum: $|J_2-J_1| \leq L \leq |J_2+J_1|$

Parity Electric: $\pi_2 \pi_1 = (-1)^L$

Magnetic: $\pi_2 \pi_1 = (-1)^{L+1}$

Table 1 lists the L-values and indicates whether there is a parity change for the first five multipoles. As an example, if there is a transition between an upper state, $J_2^{\pi} = 1/2^-$ and $J_1^{\pi} = 7/2+$, the possible L-values between the sum and difference of the two J's are just 3,4 ; and there is a parity change (Yes). Therefore, according to the table, the only possible terms in the multipole expansion are E3 and M4. A more thorough treatment of the multipole expansion can be found in standard texts. See, for example, Ref. 4.

Table 1. Parity Changes for Multipole Transitions

	E1 M1	E2 M2	E3 M3	E4 M4	E5 M5
L	1	2	3	4	5
$\Delta\pi$	Yes No	No Yes	Yes No	No Yes	Yes No

High multipole transitions occur frequently in the nuclear case but not in the atomic case. This situation arises, in part, because of the differences in atomic and nuclear structure. In the atom, electrons find themselves in the long-range coulomb field of the positive nucleus. The resulting eigenvalue spectrum has single particle levels which are filled according to the Pauli exclusion principle. This procedure gives rise to particularly stable configurations of 2, 8, 18, etc., electrons. In the nucleus, there are two types of particles which are different charge states of the same nucleon. The nucleons are bound by strong short-range forces. The forces can be approximated by a deep rectangular well. The order of the resulting levels is indicated in the left column of Fig. 5. To arrive at the empirically observed stable neutron or proton configurations at the magic numbers of 2, 8, 20, 28, 50, and 82, a spin orbit coupling term was required; the splitting increases with L and the higher J-value lies deeper. (See Ref. 5, for example.) Just below the magic numbers 50 and 82, levels with vastly different J-values are very close. Transitions between these would lead to high multipole radiation and, as we shall see below, these have very long lifetimes. They are the isomers in which we are interested. Years of empirical observation have shown that, for odd A nuclei with an odd number of either neutrons or protons, there are islands of isomerism for neutron or proton numbers just below 50 and 82. Isomers are also found in other parts of the periodic table for other reasons (e.g, shape isomers).

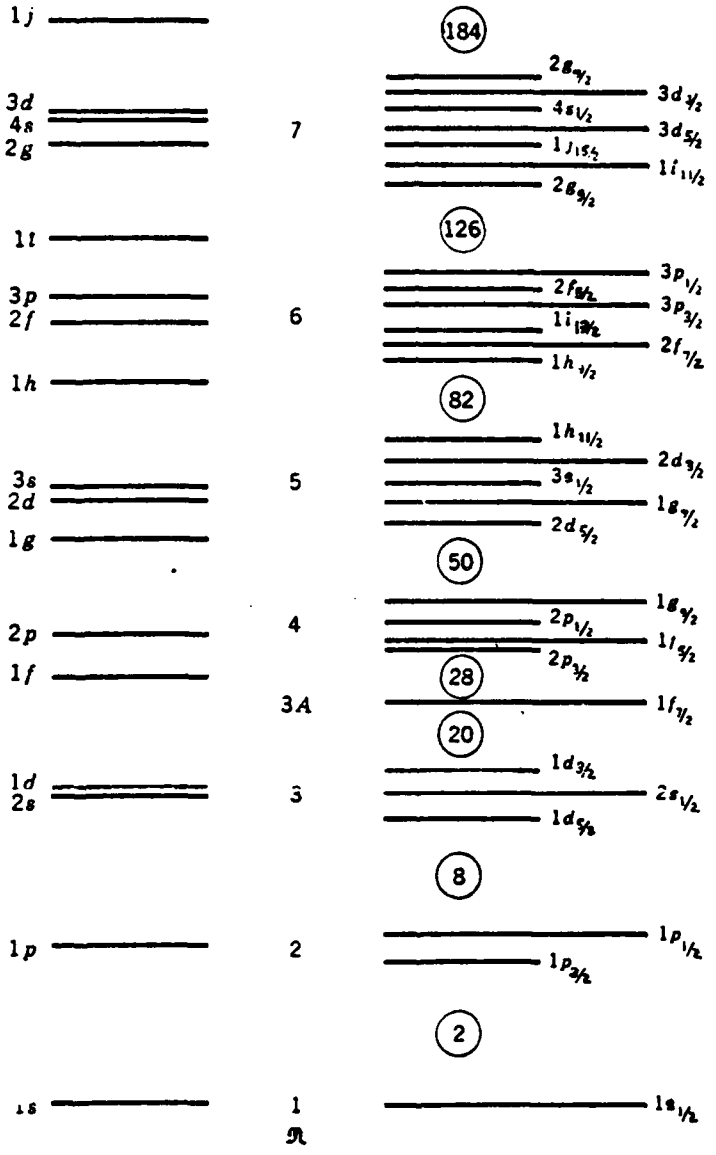

Figure 5. The nuclear shell model.

The electromagnetic lifetimes in nuclei range over many more orders of magnitude than in atoms. A highly simplified nuclear model is used by Weisskopf (Ref. 4) to estimate the lifetimes of the various multipoles over a wide range of energies. Actual lifetimes may differ from these estimates by one or more orders of magnitude. Figure 6 shows graphs of these lifetimes as a function of energy for both the electric and magnetic transitions. We are interested mainly in the region below 100 keV. Lifetimes range from about 1 fs to about 10^{20} s.

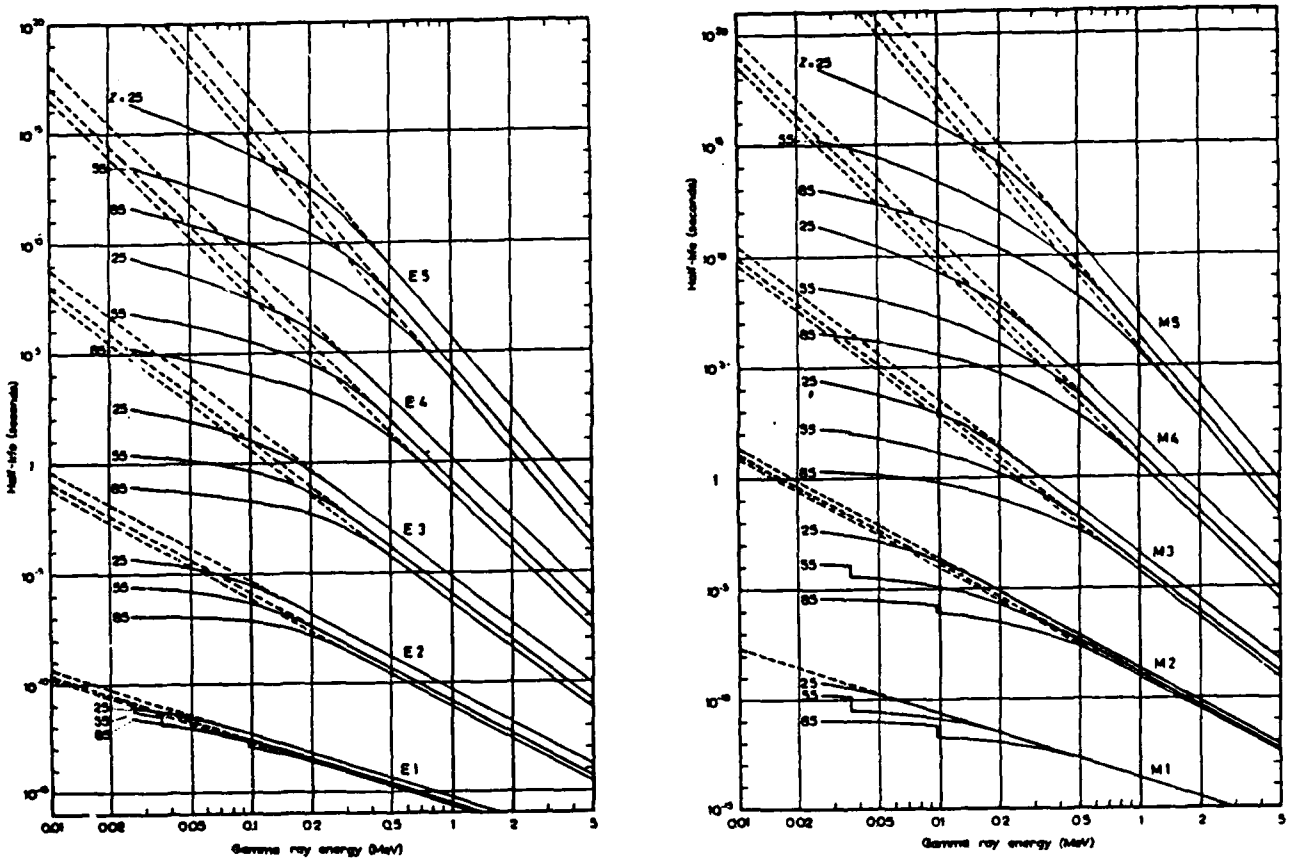

Figure 6. The half-lives of electromagnetic transitions.

C. LINEWIDTHS

The width of the transition is related to the mean lifetime by the simple transform relationship:

$$\Gamma \tau = h/2\pi, \tag{6}$$

where Γ is the full width at half maximum and τ is the mean lifetime. For a state of high excitation, a level may decay by many paths; each path has a partial width. Thus:

$$\Gamma = \Gamma_{\gamma 1} + \Gamma_{\gamma 2} + ... + \Gamma_{n} \quad \Gamma_{p} + \Gamma_{\beta-} + \quad \ldots \tag{7}$$

where each subscripted gamma is the width for the emission of that particular gamma ray or particle and the total width is the sum of all the partial widths. For a low lying state in a stable nucleus, the decay is generally entirely electromagnetic. It may take place either by gamma ray emission or by internal conversion (i.c.). In the case of a low lying state, we may write:

$$\Gamma = \Gamma_{\gamma} + \Gamma_{i.c.}\,. \tag{8}$$

Internal conversion is a process which may occur when the excitation energy of the nucleus exceeds the binding energy of an atomic electron. In such a case, the coulomb field may mediate to transfer the excitation energy to the electron and to expel that electron rather than to radiate away that energy by the emission of a photon. This mechanism is the nuclear counterpart to the Auger process in the atom. The conversion width is generally set proportional to the radiation width and is written as

$$\Gamma = \Gamma_{\gamma} + \Gamma_{i.c.} = \Gamma_{\gamma} + \alpha\Gamma_{\gamma} = (1 + \alpha)\,\Gamma_{\gamma}\,. \tag{9}$$

The internal conversion coefficient, α, is written as a series of coefficients for the various shells. Thus:

$$\alpha = \alpha_K + \alpha_L + \alpha_M + \quad \ldots \tag{10}$$

If the excitation energy is between the binding energy of the electron and the mass of the electron, there are the following simplifying approximations:

$$\alpha_K\,(E,L) \sim \frac{L}{L+1} Z^3 \left(\frac{1}{137}\right)^4 \left(\frac{2mc^2}{\hbar\omega}\right)^{L+\frac{5}{2}}$$

$$\alpha_K\,(M,L) \sim Z^3 \left(\frac{1}{137}\right)^4 \left(\frac{2mc^2}{\hbar\omega}\right)^{L+\frac{3}{2}}\,. \tag{11}$$

It is clear from these approximations that the internal conversion coefficient increases with increasing atomic number, with increasing multipolarity, and with decreasing transition energy. These effects show up clearly in the more precise computations represented in the graphs of Fig. 7. The coefficients for the L electrons are seen to have a similar functional dependence on atomic number, multipole, and energy. The internal conversion coefficient is important because it enters the formula for the stimulation cross section.

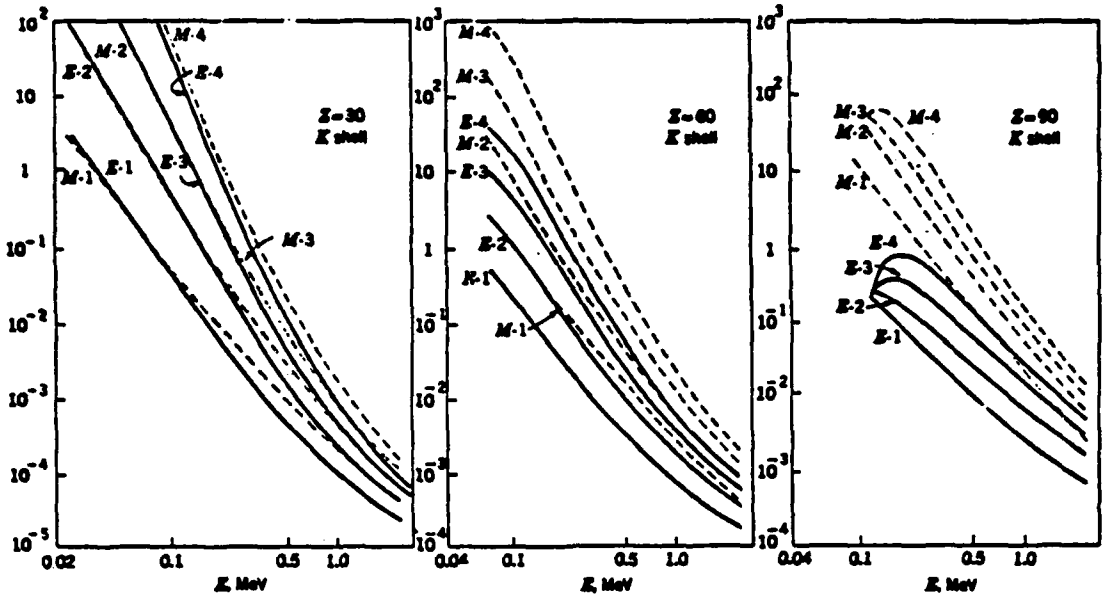

α_K, internal-conversion coefficients for K electrons, for various E-l and M-l transitions in nuclei of atomic numbers 30, 60, and 90. *(From C. M. Lederer et al., "Table of Isotopes," Wiley, New York, 1968; by permission.)*

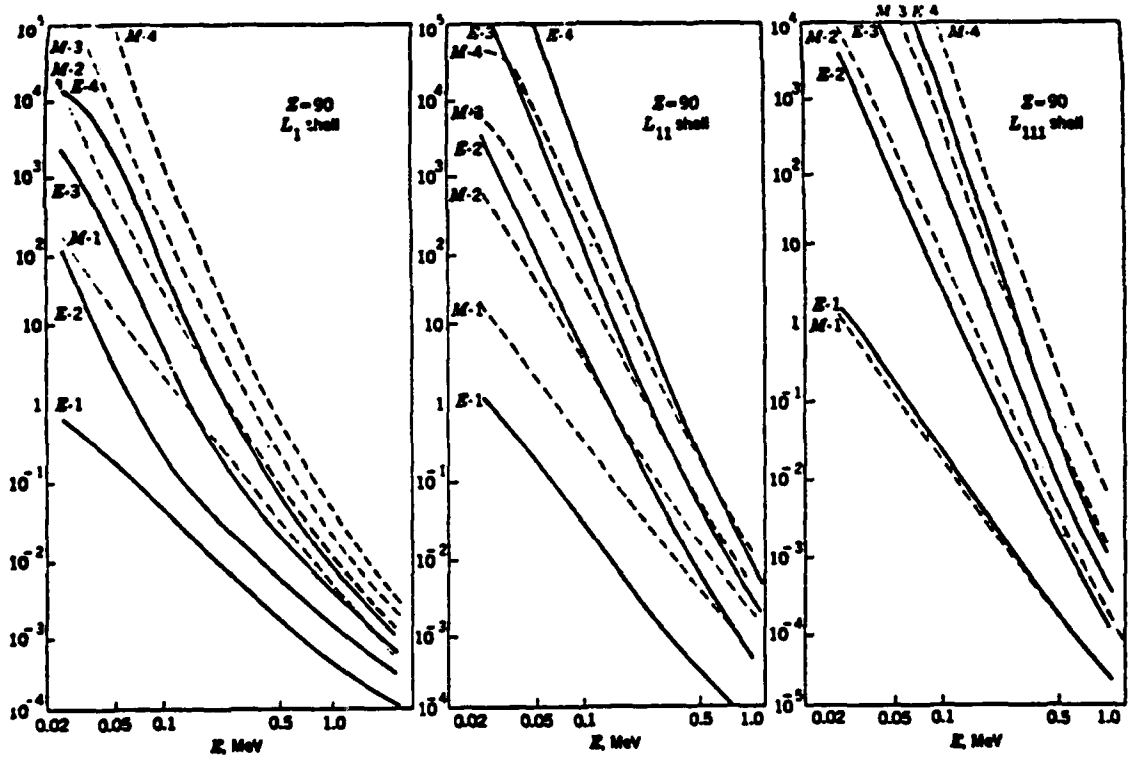

Figure 7. Internal conversion coefficients for various multipole transitions in nuclei of atomic numbers 30, 60, and 90.

D. CROSS SECTIONS

Consider transitions between the two levels shown in Fig. 4. For absorption, the cross section can be obtained from the single level Breit-Wigner formula and is given by:

$$\sigma_{abs} = \frac{2J_2 + 1}{2(2J_1 + 1)} \frac{\lambda^2}{\pi} \frac{\Gamma_\gamma}{\Gamma} \frac{1}{1+x^2}, \qquad (12)$$

where

$$x = (E - E_o)/(\Gamma/2) .$$

The stimulation cross section (as in the atomic case) is obtained from a comparison of the Einstein B coefficients. It is given by:

$$\sigma_s = \frac{2J_1+1}{2J_2+1} \sigma_{abs} = \frac{\lambda^2}{2\pi} \frac{1}{1+\alpha} \frac{1}{1+x^2} = k\lambda^2 \frac{1}{1+x^2} . \qquad (13)$$

A number of factors affect the emission and absorption spectra of the two-level system. These include recoil of the absorbing or emitting nucleus and Doppler shifts of frequencies due to the Maxwellian distribution of velocities of the atoms.

Recoil is important in the nuclear case because the natural widths of the transitions that we shall consider will, in many cases, be very narrow. The emitting nucleus yields a photon whose energy is the transition energy minus the recoil energy, E_R. On the other hand, the absorbing nucleus, in its ground state, must receive a photon whose energy equals the transition energy plus the anticipated recoil energy. Thus, the peaks of the emission and absorption spectra are separated by twice the recoil energy. These conditions obtain for nuclei in the atoms of a gas at 0 K. If the gas is raised to the temperature T, the widths of the lines are Doppler broadened. The situation is depicted in the sketches of Fig. 8. The Doppler width in a gas is given by

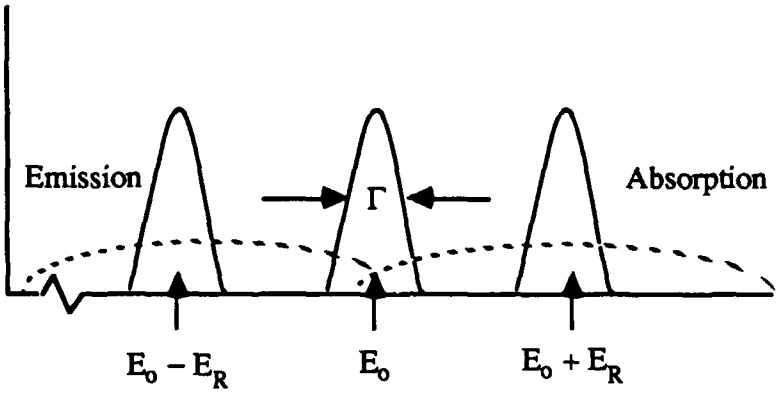

Figure 8. Emission and absorption spectra for stationary nuclei. The dotted curves represent the Doppler-broadened spectra for nuclei at the temperature T.

$$\Delta = E_o \sqrt{\frac{2kT}{Mc^2}} \, . \tag{14}$$

(Ref. 6) If the atoms are located in a solid lattice, the expression is modified to:

$$\Delta = E_o \sqrt{\frac{2kT_{eff}}{Mc^2}} \, , \tag{15}$$

(Ref. 7), where T_{eff} is given by

$$T_{eff} = T\, f\left(\frac{\Theta}{T}\right) = T\left[\frac{C_v\left(\frac{\Theta}{T}\right)}{24} + \frac{3\left(\frac{\Theta}{T}\right)}{4\left(e^{\Theta/T} - 1\right)} + \frac{3\left(\frac{\Theta}{T}\right)}{8}\right] . \tag{16}$$

where C_v is the specific heat and Θ is the Debye temperature.

Generally, $\Delta >> \Gamma$, and the cross section for absorption (or stimulation) becomes:

$$\sigma(E) = \sqrt{\frac{\pi}{2}}\ \frac{\Gamma}{\Delta}\ \sigma_o \exp - (\Gamma x/2\Delta)^2 \, . \tag{17}$$

Recoil and broadening effects are compared for a typical atomic transition and two Mössbauer nuclei. The results are shown in Table 2. It is obvious from the last column that the stimulation cross section can be diminished many orders of magnitude by Doppler broadening.

Table 2. Recoil and Broadening Effects

	λ (cm)	E_0 (eV)	Γ_γ (eV)	2Δ (eV)	$2E_R$ (eV)	$\Gamma/2\Delta$
Na Atom	5.9×10^{-5}	2.1	4.5×10^{-8}	(300K) 6.6×10^{-6}	2×10^{-10}	0.007
^{191}Ir	9×10^{-10}	129k	4.7×10^{-6}	0.14	0.09	3.4×10^{-5}
^{57}Fe	8.6×10^{-9}	14.4k	4.6×10^{-9}	0.02	0.004	2.3×10^{-7}

In order to achieve gain in a pumped medium, the Schawlow-Townes relationship (Ref. 8) requires that:

$$(N_2 - g_2N_1/g_1)\sigma_{stim} > \sum N^i\sigma^i_{nr} \ , \tag{18}$$

where the N's and the g's are the populations and degeneracies of the respective levels. The σ's are the stimulation and non-resonant cross sections. The stimulation cross section is given by:

$$\sigma_{stim} = \frac{\lambda^2}{2\pi} \ f \ \frac{1}{1+\alpha} \ \frac{1}{1+x^2} \ , \tag{19}$$

where f is the Mössbauer fraction, i.e., the fraction of emissions or absorptions for which the entire recoil is taken up by the crystalline lattice. In Table 3, we compare the various cross sections at a range of energies. The stimulation cross sections exceed the non-resonant cross sections; however, it should be noted that in a real situation, the stimulation cross section would be reduced many orders of magnitude by a combination of factors such as internal conversion, Mössbauer fraction, Doppler broadening, and crystalline inhomogeneous broadening.

Table 3. Cross Sections

E_o	λ	$\frac{\sigma_o}{k} = \lambda^2$		σ_{photo}		$\sigma_{compton}$	
				S_n	P_b	S_n	P_b
1.2 keV	10Å	10^{10} b		1.5×10^6	2×10^6	1.5×10^3	4×10^3
12	1	10^8		2×10^4	3×10^4	5×10^2	2×10^3
120	0.1	10^6		300	2×10^3	40	100

$$k = [2\pi(1+\alpha)]^{-1}$$

E. STIMULATION SYSTEMS

Assume that, as in Fig. 9, we have a black box containing an electromagnetic system. The box is black only in the visible so that we cannot see into it. The system is a two-level system, capable of being excited into the upper state by absorbing a photon of energy $h\nu_a$, and of spontaneously decaying from the upper state to emit a photon of energy $h\nu_e$. If the system is in the upper state and a directed wave of energy $h\nu_e$ passes over it, the system may be stimulated to emit a photon of energy $h\nu_e$ having the same linear and angular momenta as the stimulating photon. What kind of stimulatable systems can we find to put into the black box? We shall describe two systems.

First, consider a two-level nucleus in an atom at rest. If the nucleus is in the upper state, it can emit a photon of energy $(E_o - E_R)$, i.e., the transition energy minus the recoil energy. The excited nucleus can, therefore, also be stimulated to emit that photon by a directed photon of the very same energy $(E_o - E_R)$. However, a nucleus in the lower state cannot absorb a photon of this energy; it can only absorb a photon of energy $(E_o + E_R)$. A good system is therefore a gas of stationary atoms with a fraction of the nuclei in the excited state. Let us consider only those processes occurring in a direction parallel to the main axis of the acicular shape. Any spontaneously emitted photon can stimulate the emission of another photon. A stationary nucleus in the lower level requires a photon of energy $(E_o + E_R)$ to be excited to the upper state. An atom whose nucleus has just been stimulated by a stream of photons of energy $(E_o - E_R)$ is in the lower level and is recoiling with the energy E_R towards the streaming photons with laboratory energy $(E_o - E_R)$. To

absorb a photon and be reexcited into the upper state, the nucleus would have to encounter a photon of laboratory energy E_0. There are none. There are thus no nuclear nonresonant processes. In this sense, the nuclear case differs from the atomic. Again, a viable system is a gas of atoms or molecules at rest, with each atom or molecule containing the candidate nucleus. Another system is a gas whose constituents are all moving with the same speed, v; we need merely to transform to a frame of reference in which all the atoms or molecules are at rest and the previous situation will again obtain. In other words, one needs a system whose constituent particles have a velocity distribution which is a delta function.

The second example is merely another way of achieving a delta function velocity distribution. The atom is now made part of a strongly bound crystalline lattice. When its nucleus emits, the recoil is taken up by the entire crystal, not by the individual atom. The recoil is therefore negligible. In other words, we require a solid whose nuclear emitters undergo a Mössbauer effect. Thus, both systems effectively have a delta function velocity distribution. However, there is one difference. In the gas case, the resonance energy for stimulation is $(E_0 - E_R)$, and for absorption, $(E_0 + E_R)$. An excited state population larger than the ground state population is not required for gain. In the Mössbauer case, stimulation and absorption occur at the same energy, E_0; and, therefore, inversion is required.

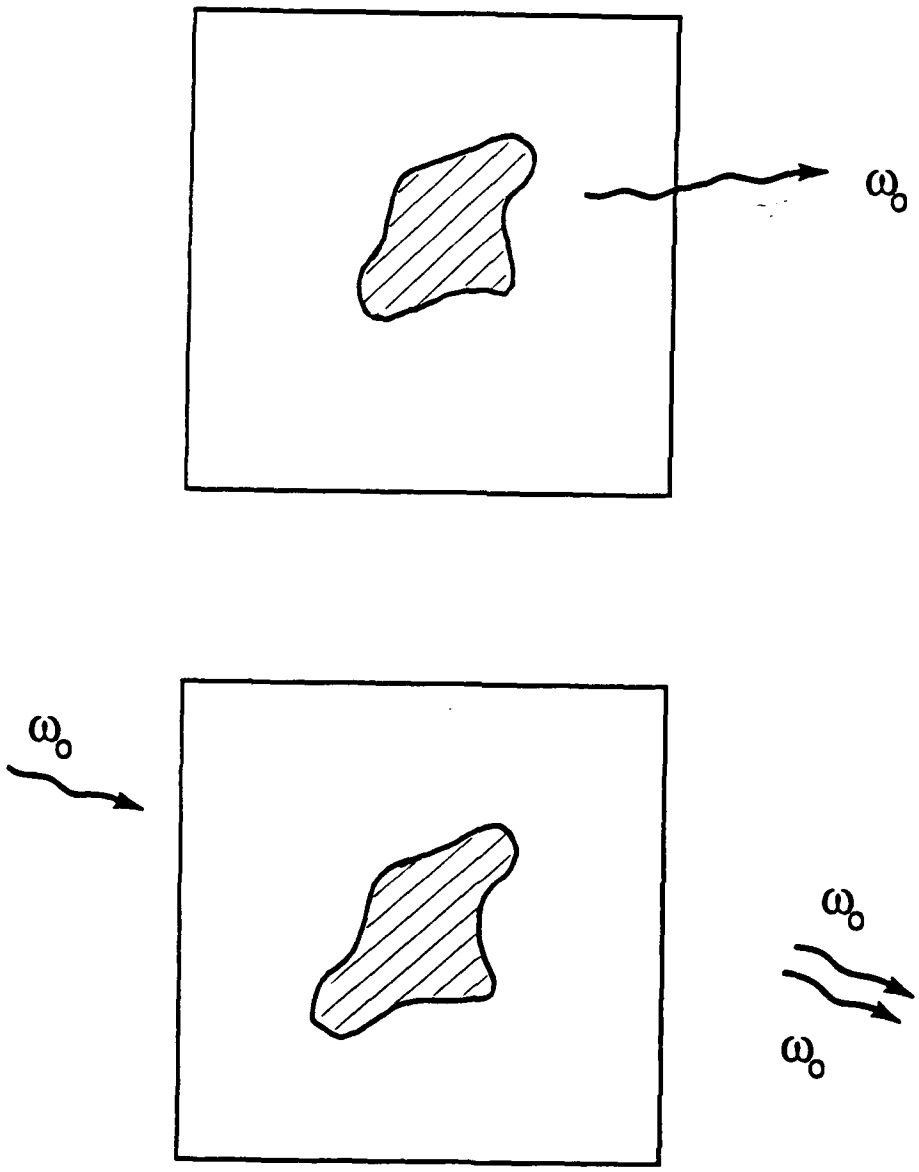

Figure 9. Spontaneous and stimulated emission from an electromagnetic system contained in a black box.

F. THE GAS GRASER

Two velocities immediately suggest themselves - zero and c, the speed of light. The first, because it is achieved by going to 0 K; the second, because it is the upper limit against which high-energy accelerators squeeze the velocity distribution.

1. The Velocity Zero.

In 1975, Hansch and Schawlow (Ref. 9) suggested that the atoms of a gas could be slowed down to zero by irradiating the sample of gas from all six directions with a laser tuned to the low-frequency edge of a Doppler-broadened resonance line. Atoms moving towards the laser will see its photons Doppler-shifted towards resonance. Each absorption will cause the atom to lose an amount of momentum equal to the momentum of the photon, $h\upsilon_C$. The authors calculated that with a 2852 Å laser, a sample of magnesium gas could be cooled from 600 K to 0.24 K in 30 μs. In 1983, using only one laser beam and a counterflowing beam of sodium atoms, several groups (Refs. 10 and 11) achieved a stationary sample of gas with temperatures of the order of 50 mK. Refinements of this technique at the National Bureau of Standards (NBS) and AT&T Bell (Ref. 12) have recently led to samples of sodium gas at temperatures of about 1 mK.

Let us now consider a gas sample of molecules (mass M) having a nuclear constituent with the transition of interest characterized by the energy E_N and the lifetime τ_N. The molecule also has an atomic (or molecular) transition which is the cooling transition; it is characterized by the transition energy and lifetime E_C and T_C, respectively. Let us assume that we are laser-cooling from a temperature T to 0 K. At T, the mean velocity of a molecule is:

$$V = \left(\frac{3\,kT}{M}\right)^{1/2} . \tag{20}$$

The decrease in velocity due to the absorption of one photon of momentum ΔP is given by

$$\Delta V = \Delta P/M = E_C/Mc . \tag{21}$$

The number of absorptions to cool is therefore:

$$N_C = V/\Delta V = (3Mc^2KT)^{1/2}/E_C . \tag{22}$$

where c is the speed of light. One may either pump the graser (or gamma-ray laser) first and then cool, or cool and then pump. Assume we pump first. Then, in cooling, assume

the atomic transition is pumped to saturation. Then, on the average, there is one absorption every T_C. The time to cool is then given by the number of absorptions times the time for one absorption, or

$$\text{Time To Cool} = N_C\, T_C\,. \tag{23}$$

To be effective and not lose the population inversion, the nuclear lifetime should obey the relationship

$$\tau_N > N_C\, T_C\,. \tag{24}$$

Given the parameters

$T = 300K$,

$M = 250$, and

$E_C = 1$ eV,

we obtain

$$\tau_N > 1.3 \times 10^5\, T_C\,.$$

For $T_C \cong 10^{-8}$ s, we get:

$$\tau_N > 10^{-3}\ \text{s}\,.$$

This situation could be a severe constraint on the graser design. However, if we cool first and then pump, the problem may be resolved. Ultimately, the resolution depends on how closely the temperature approaches 0 K.

2. The Velocity c.

A high-energy accelerator takes a particle from an energy Mc^2 to an energy γMc^2 where

$$\gamma = (1 - \beta^2)^{-1/2}\,,$$

and

$$\beta = V/c\,. \tag{25}$$

The spread in energy is given by

$$\Delta E = (\Delta\gamma)\, Mc^2\,. \tag{26}$$

The velocity spread is given by:

$$\Delta\beta = (1/\beta)\,(\Delta\gamma/\gamma^3) = \Delta\gamma/\gamma^3 \qquad (27)$$

since $\beta \rightarrow 1$ for relativistic particles. In the reference frame of the beam, this expression becomes

$$\Delta\beta' = \Delta\gamma/\gamma = \Delta E/E. \qquad (28)$$

In order to achieve a laser, the sample has to be cooled to the point where:

$$\Gamma_D \sim \Gamma_\gamma$$

or

$$\Delta\beta' E_o \cong \Gamma_\gamma\,. \qquad (29)$$

For a 50 keV transition with $T_N = 10^{-8}$ s

$$\Delta\beta' \cong 10^{-12}\,,$$

i.e.,

$$\Delta V' \cong 0.03 \text{ cm/s}.$$

For current accelerators, the energy spread is many orders of magnitude away from the above figures. For example

Van de Graaffs [5 MeV]	$\Delta\beta' = \Delta\gamma/\gamma \cong 10^{-5}$
Michigan State University Cyclotron [15 MeV protons]	10^{-3}
Bevelac [1 - 2 GeV/nucleon]	$\lesssim 10^{-2}$

(Ref. 13). Thus, of the two velocities, zero seems the more viable.

G. THE MÖSSBAUER SOLID

A group of stationary nuclei will display the usual Lorentzian shape for an absorption or stimulation resonance, namely,

$$\sigma = \sigma_o\,(1 + x^2)^{-1}. \qquad (30)$$

If the nuclei are in a solid, there is a Maxwellian distribution of velocities, with the consequent Doppler broadening of the resonance. The formulae now take the shape

$$\sigma = \frac{\sqrt{\pi}}{2}\ \xi\ \sigma_o\ \exp\left(-\xi^2 x^2/4\right), \tag{31}$$

where

$$\xi = \Gamma/\Delta << 1,$$

and

$$\Delta = E\,(2kT_{eff}/Mc^2)^{1/2},$$

and T_{eff} is a function of (Θ/T) and Θ is the Debye temperature. This effect, coupled with recoil, gives the absorption and emission spectra shown in Fig. 10.

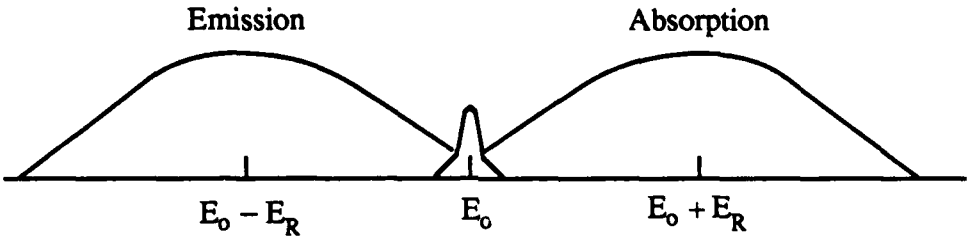

Figure 10. Doppler-broadened emission and absorption spectra.

The peaks of the emission and absorption spectra are separated by the energy interval $2E_R$. At E_o, there is a sharp peak in each spectrum that is due to the fraction of nuclei that undergo emission or absorption with no individual recoil but have the recoil taken up by the entire lattice. This fraction is given by the Debye-Waller factor

$$f = \exp(-2W) = \exp\left[-\frac{3E_R}{2k\Theta}\left\{1 + \left(\frac{T}{\Theta}\right)^2 \int_0^{\Theta/T} y\,(e^y - 1)^{-1}\,dy\right\}\right]. \tag{32}$$

The fraction can approach unity for low-energy transitions in heavy nuclei embedded in lattices with high Debye temperatures. All the current lasing schemes demand a Mössbauer effect. The experimental Mössbauer regime is approximately in the lifetime region from 10^{-8} to about 10^{-4} s. That region is being extended towards longer lifetimes. The cross section has the form:

$$\sigma_{stim} = (g_1/g_2)\,\sigma_o f\,[1 + x^2]^{-1}. \tag{33}$$

Sometimes an additional factor is applied to take into account the broadening due to the inhomogeneities in the crystal.

H. PRESENT APPROACHES TO THE GRASER

The three major approaches at present are depicted in Fig. 11. All begin with the nuclei in a long-lived isomeric state.

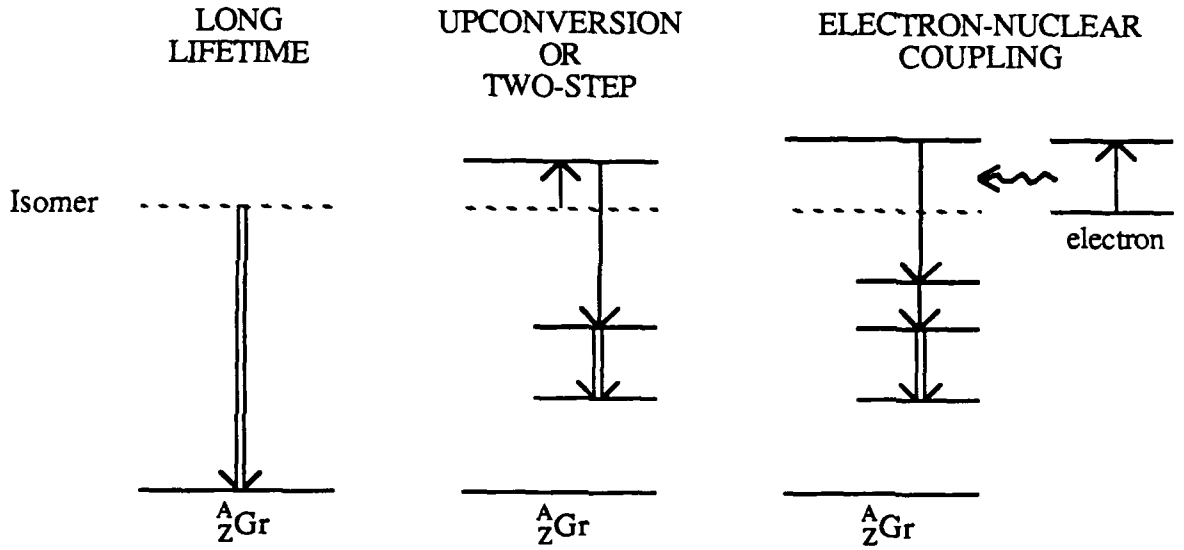

Figure 11. The three major pumping schemes.

In the first approach, the isomer itself is used as the upper state of the lasing pair. Because of its lifetime, given that

$$\Gamma\tau_N = 6.58 \times 10^{-16} \text{ eV-s}$$
$$= 0.159 \text{ Hz-s}, \qquad (34)$$

the radiation width is very narrow. In general, the inhomogeneities of the crystal greatly broaden the width and thereby reduce the effective cross section by many orders of magnitude. One scheme is to use nuclear magnetic resonance (NMR) techniques to remove the inhomogeneities. Other techniques are being proposed.

In the second approach, it is assumed that there is a level nearby which can be reached from the isomer by either a laser or an x-ray source. This level has a short lifetime and cascades down to the upper state of the lasing pair.

A two-step process is involved in the third approach. First, one must excite the electron cloud surrounding the nucleus. Then, given compatible electronic and nuclear

level structures, the electronic excitation transfers to the nucleus. Again, either the upper level of the cascading pair has been reached, or there is a cascade to it.

I. GENERAL GRASER PROBLEMS AND NEEDS

If one were to do a systems study leading to the actual design and construction of a graser, many studies would have to be undertaken and many questions resolved. Among them are the following:

1. **Data Bases** - Nuclear data bases specific to the needs of the various pumping schemes need to be constructed. Some are in process or completed. (e.g., Ref. 14)

2. **Producing Macro Samples of Isomers** - as experiments are proposed, samples of specific long-lived isomers will need to become available in sufficient amounts to make crystals.

3. **Crystal Fabrication** - high-purity, defect-free crystals will be needed. They will have to be very homogeneous and acicular in shape. It may be necessary to implant the desired nuclei in a host lattice. Implanting will have to be substitutional. Crystalline planes will have to be oriented to produce Bragg scattering within the crystal to enable the establishment of Borrmann modes.

4. **Radiation Damage** - the crystal will contain a high density of radioactive nuclei. Spontaneous decay of these nuclei may produce enough damage to the lattice to decrease the Debye-Waller factor and to produce inhomogeneous broadening. These effects need to be studied.

5. **Lattice Heating** - in the process of pumping the isomer, enough heat may be generated in the crystal to either destroy the Mössbauer effect or to melt the crystal itself. These effects are being investigated. (See Chapter II.)

6. **Superradiance** - many investigators assume that the graser will be a superradiant device. Studies should be conducted to determine whether the conditions required for superradiance can be achieved.

J. SCHEME-SPECIFIC PROBLEMS

Each lasing scheme brings with it its own characteristic problems:

1. Long Lifetime

- Mössbauer Effect - Achieving the effect for long-lived transitions has been extremely difficult. Experiments must be carried out, preferably using candidate nuclei.
- Inhomogeneous Broadening - The rapid suppression of this broadening is required to trigger the energy release in this scheme. Demonstration experiments should be undertaken in the not too distant future.
- Internal Conversion - A long lifetime implies a high multipolarity which, in turn, implies a large internal conversion coefficient.

2. Upconversion

- Candidate - Finding a candidate with a suitable sequence of nuclear levels may present a very difficult problem. If one cannot be found in searches using the current nuclear compilations, theoretical studies combined with limited experimental searches will have to be carried out.
- Pumping - Laser pumping (especially for $\lambda > R_{atom}$) may encounter extreme difficulties due to both the impenetrability of the electron cloud and to lattice heating.

3. Electron - Nuclear Excitation

- Electron Excitation - The excitation of the electron cloud may require the deposition of sufficient energy to destroy the lattice. Experimental demonstrations are needed.
- Atomic and Nuclear Spectra - The eigenlevel structure of nucleus and electrons must be compatible to enable the transfer of excitation. Here again, a mixture of theory and experiment may be essential.
- Mössbauer Effect - The ability to maintain the effect despite the deposition of large amounts of energy during the excitation process must be investigated.

II. HEATING DURING UPCONVERSION IN A GAMMA-RAY LASER

A. INTRODUCTION

It has long been hoped that very short wavelength lasers can be built by using nuclear transitions to provide the photon (Ref. 15). Because of the large energies involved, it has been proposed to store energy in an isomeric state, and release it in a single pulse by upconverting to a lasing transition (Ref. 16). (See Fig. 11 of this report.) It is the purpose of this note to examine the heating of a sample material during such an upconversion with X-rays. Heating is a serious concern for a gamma ray laser because, unlike the situation with X-ray lasers, the Mössbauer effect will be needed to keep the photons and excited states in resonance. The examination will focus on the heating of an ^{57}Fe sample during excitation of the Mössbauer state at 14.4 keV. The arguments and physical trends do not extend to the visible and near UV regime. These will be examined in a separate paper.

To indicate how serious heating will be during upconversion of nuclear levels we express the law of DuLong and Petit for specific heat capacities of metals in unconventional units. The standard value of 25 J/mole-K converts to 2.6×10^{-4} eV/atom-K. This means that during upconversion with 10 keV photons, an energy leakage of ten parts per million going into thermal channels would raise the temperature of the sample by 400 K. To raise iron from absolute zero to the liquid state would require less than 65 parts per million. Resonant cross sections will be large, but nearly all the absorption must be by the nuclear transition in order not to melt the material.

In the second section of this paper we outline the calculation, and define the needed parameters for the case of ideal beam--one which is of zero width and exactly tuned to the excitation energy. Even this favorable assumption leads to damaging heating, except for samples that are very thin compared to the radiation length of resonant photons. Such thin samples would lead to inefficient use of the upconversion photons and increase pump power requirements.

For non-ideal triggering beams the situation is worse, because finite beam width will enhance the photoelectric effect relative to the resonant excitation. Expected heating as a function of beam width is presented in Section C, along with expected trends for variation in upconversion energy and atomic number. The results indicate a serious problem which would require orders of magnitude increases in both beam intensity and resolution.

It has been suggested that these problems can be dealt with by conductive cooling, (Ref. 17) or by triggering the laser in a time short compared to the crystal disintegration time (Ref. 18). These ideas are discussed in Section D, along with some preliminary results. Conclusions are presented in Section E.

B. SAMPLE CALCULATION--^{57}FE

In this section we compute the heating during upconversion from the ground state to the 14.4 keV state in ^{57}Fe. We assume that the incident radiation is exactly on resonance and neglect any detuning, and do not include any effects of heating due to decay of the excited state. For the case calculated, there is no alternate decay channel except back to the ground state, and a relatively small internal conversion coefficient. This approach results in a very favorable case from the point of view of heating.

The essential ingredients in this calculation are the resonance cross section for upconversion of the desired state, the competing photoelectric cross section, along with the energy loss cross sections for the resulting electrons, and finally the geometry of the sample. Knowledge of the basic bulk properties of iron is also needed. First we assume that the nuclear excitation is exactly on resonance. The cross section for excitation-de-excitation is:

$$\sigma_R = \frac{\lambda^2}{2\pi} \frac{\Gamma_e \Gamma_i}{(\Gamma_T)^2}, \tag{35}$$

where λ is the wavelength, and the Γ's are the elastic (Γ_e), inelastic (Γ_i) and total widths (Γ_T). For the case under consideration here, simple upconversion to a state which only decays back to the ground state, the cross section simplifies to:

$$\sigma_R = \frac{\lambda^2}{2\pi} \frac{\Gamma_e}{\Gamma_T}. \tag{36}$$

The ratio of widths is often written $1/(1+\alpha)$, where α is the internal conversion coefficient. This is the ratio of internal conversion to photon emission decays of the state. For the case under consideration, the resonant cross section is 2.38 Mb (Ref. 19). The competing

photoelectric cross section is only about 7000 b, (Ref. 20) or 200 times smaller. The corresponding radiation lengths (L_x) defined as the reciprocal of the linear extinction coefficient, are given in Table 4.

Table 4. Radiation lengths associated with resonance excitation, photoelectric effect and high energy (14 keV) electron loss in ^{57}Fe.

^{57}Fe	1/L (A^{-1})	L (μm)
σ_R	1.11E-03	0.0899
σ_{PE}	5.94E-06	16.8
$(dE/dx)_e$	7.90E-05	1.27

To compute the heating associated with a given level of upconversion it is necessary to know the probability of photoelectron emission as a function of the probability of resonance excitation. Because excitation of the resonant state removes potential targets from future photons, the relative effectiveness of the photoelectric process increases as the population is inverted. The correct expression for the total probability of photoelectron (P_{PE}) emission as function of the final fraction of nuclei in the resonant state (P_R) is

$$P_{PE} = \frac{L_R}{L_{PE}} \ln\left[\frac{1}{1-P_R}\right].$$

This in an important correction for $P_R = 0.5$ or greater.

The next physical parameter that is needed is the average energy deposited in the material per photoelectron. This energy comes from two sources. First, the photoelectron itself deposits energy on its way out. Second, the residual excited atom decays either by electromagnetic or Auger processes, and these electrons and photons deposit energy. In order to ensure that the heating was not being overestimated, we assumed that the photo-effect produced a high-energy electron and left relatively little energy behind in the excited atom. Since energy loss per unit length increases rapidly as the electron slows down, assuming a high energy photoelectron underestimates the calculated energy deposition, provided the sample is small enough that the photoelectrons escape.

This assumption of an energetic electron also leads to a minimal contribution to heating from the atomic excitation, since relatively little energy is deposited. To characterize this numerically we have taken the effective energy absorption cross section to be 1Mb, which is the cross section of 100 eV photons in carbon (Ref. 21). We expect this assumption to underestimate the true absorption. To turn this number into a rough energy deposition, we compute $E_{ATOM} = P_{PE}\, E^*[1 - \exp(-a/2L)]$ where E^* is the excitation energy of the atom (the incident x-ray energy minus the ejected electron's energy) and a is the radius of the wire. The energy deposition per atom estimated in this fashion is given in Table 5.

The energetic photoelectron will have a range in the material which varies as the energy squared. In other words, it loses energy progressively more rapidly as it slows down. This is observed empirically and the trend persists down to energies on the order of 100 eV. We obtain a lower limit on the energy deposition by linearizing the energy loss. For photoelectrons uniformly produced in a long cylinder, with isotropic velocities, the angle averaged distance to travel to the edge of the cylinder, s, increases from the radius for particles at the edge to $\pi/2$ times the radius for particles at the center. We can compute a lower limit on the energy deposited by the photoelectron by using the minimum value of s, along with a radiation length associated with the initial energy of the particle to write

$$E_{PE} = P_{PE} \frac{dE}{dx} s_{min} .$$

Since photoelectrons are preferentially produced perpendicular to the direction of motion of the incident photon, the assumption of isotropy further decreases the estimated energy deposition. We hope to remove these approximations in order to get a more reliable estimate. At the moment it is worth noting that our present "estimate" is in fact a very conservative lower bound. The energy depositions from the energetic electrons are also given in Table 5 for a variety of iron wire thicknesses, along with the total values from both contributions. Also shown is the final temperature of the sample, assuming an initial temperature of 100 K, and a heat capacity from the Law of DuLong and Petit. This serves to make the numbers roughly applicable for any metal.

Now let us consider the consequences of the results in Table 5. For a variety of radii of iron wire (first line) we have computed the effective absorption probability (second line). All calculations assume an incident photon number equal to the number of atoms in the sample. The fraction of the sample upconverted increases with thickness, but somewhat slower than linearly. The fraction of photons which convert to photoelectrons

increases linearly. The photoelectric energy deposition is approximately quadratic in the thickness. The final temperature increases dramatically with sample thickness as shown in Fig. 12. A cold (100 K) sample of thickness 0.01 μm would not heat up to room temperature; however, doubling the thickness to 0.02 μm results in a final temperature

Table 5. Heating as a function of whisker thickness for ^{57}Fe. In all calculations the fluence is scaled so that the photon number equals the number of atoms in the sample.

a (μm)	0.01	0.0201	0.032	0.036	0.0375	0.04	0.05	0.0625
P_R	0.11	0.20	0.30	0.33	0.34	0.36	0.43	0.50
P_{PE}	0.0006	0.0012	0.0019	0.0021	0.0022	0.0024	0.0030	0.0037
DEPOSITION FROM PHOTO-ELECTRON (eV)	0.03	0.13	0.34	0.43	0.47	0.53	0.83	1.29
DEPOSITION FROM ATOM (eV)	0.01	0.06	0.15	0.19	0.20	0.23	0.36	0.57
TOTAL	0.05	0.19	0.49	0.62	0.67	0.76	1.19	1.86
TF	283	840	1810	1836	1945	2137	3030	4425
E-OUT (mJ)	0.02	0.16	0.60	0.84	0.984	1.12	2.08	3.82

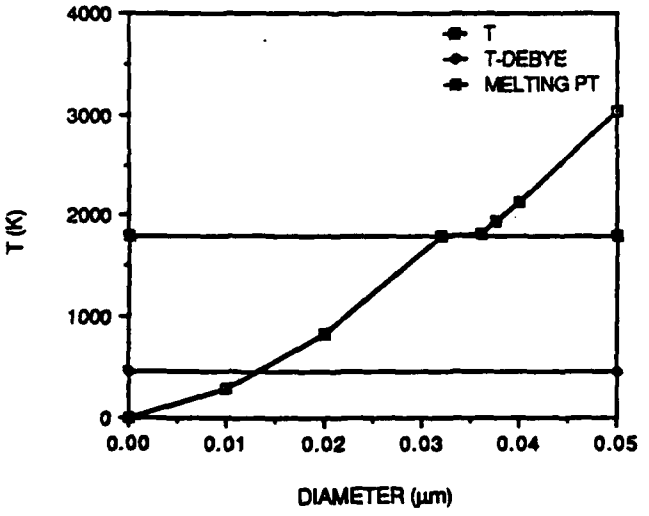

Figure 12. Temperature increase with whisker thickness for perfectly on-resonance beam

of 840 K, which is almost twice the Debye temperature. By 0.03 μm the sample has begun to melt.

There are two difficulties with avoiding heating by going to very small samples. First, one would have difficulties in preparation. Second, the energy stored becomes very small. It is certainly true that using nuclear energy levels allows very efficient storage of energy, but if only a small fraction of a small sample can be triggered, then there might be no practical applications. Table 5 also gives the released energy, assuming the given conversion efficiency. We see that very small energies are involved, small even compared to a single pulse from a conventional pulsed laser.

C. UPCONVERSION WITH FINITE WIDTH BEAMS

The effect of finite beam width on the upconversion process is to make the effective resonance cross section smaller, while leaving the photoelectric process essentially unchanged. Synchrotron radiation may be used to provide well resolved X-rays in the 1 to 10 keV energy range, with beam widths on the order of 0.1 eV, and intensities of 5×10^8 photons per burst. These pulses would typically last around 20 ns, with a pulse repetition frequency of 1000 Hz.

In order to effectively upconvert a nuclear state, one needs a lifetime long compared to the length of the burst, and an intrinsic width large compared to the beam spread. Since a 10 ns lifetime corresponds to a 6.6×10^{-8} eV intrinsic width, and these quantities have a reciprocal relationship it is impossible to simultaneously meet both requirements with current beams. Recently, a very high resolution (0.005 eV) measurement was reported, (Ref. 22) but this resolution improvement came at the cost of greatly reduced intensity, as is usually the case. The most noteworthy features of these beams are that they are broad compared to the width of the state, they are not intense enough, and finally there are relatively few photons within one natural linewidth.

In the case of upconversion with a broad beam, it is necessary to account for the decreased effective resonance cross section. In general, it is also necessary to account for "bleaching" of the beam, i.e., preferential removal of photons from the resonance peak, but for very thin samples as considered here, this effect can be neglected. For large beam spread ΔE compared to the width of the state, the average cross section varies like

$$\bar{\sigma} \sim \sigma_o \frac{\Gamma}{\Delta E} .$$

The $1/\Delta E$ dependence is due to the factor normalizing the beam to fixed intensity. The constant of proportionality depends on the functional form used to represent the beam shape. Differences in this constant are small. We used a uniform energy distribution of total width ΔE, which gives for the effective cross section

$$\bar{\sigma} = \sigma_0 \frac{\Gamma}{\Delta E} \arctan\left(\frac{\Delta E}{\Gamma}\right).$$

The effect of finite beam width is shown in Fig. 13, where the energy deposition in ^{57}Fe is plotted as a function of the ratio of beam spread to natural width. The target wire is assumed to have a 0.01 μm diameter. The upconversion was set at 1 percent of the sample. This is the minimum consistent with gain during stimulated emission. The arrow indicates the ratio appropriate for a 0.1 eV width and a state with a 10 ns lifetime. It is clear that there is too much energy deposition by orders of magnitude.

It has long been recognized that the Borrmann effect would be needed to reduce the heating through atomic scattering. An optimistic assessment might anticipate a factor of 100 suppression of the photoelectric cross section. The calculations were repeated assuming such a suppression, and the results are presented in Fig. 14. Even under these circumstances, with current resolution, nearly 100 times the energy necessary to melt the sample would be deposited in the process of upconverting 1 percent of the nuclei.

The energy of the calculation was chosen from the observed transition. We can ask, what would the heating be for a lower energy X-ray transition? Naively, one might expect decreased energy deposition, but in fact the opposite results. With softer X-rays, the photoelectric cross section increases dramatically, generally scaling as $1/E^4$. The resonance cross section, meanwhile, will not change much at the peak because of internal conversion. The factor α from the ratio Γ_e/Γ_T in equation (36) increases like λ^2, hence the peak cross section is essentially constant. To make matters worse, the width of the state decreases as the energy of the transition decreases. This means that for fixed resolving power, the ratio of $\Delta E/\Gamma$ will increase with lower energy. (This change in width is not included in the calculations presented here, since results are shown as a function of $\Delta E/\Gamma$.) In addition to lower energy x-rays producing more photoelectrons, the resulting low energy electrons lose their energy faster on the way out of the material.

Expected heating of an iron-like material by 1 keV upconverting photons is shown in Fig. 15 for the same target whisker as above. A beam width equal to a few times the

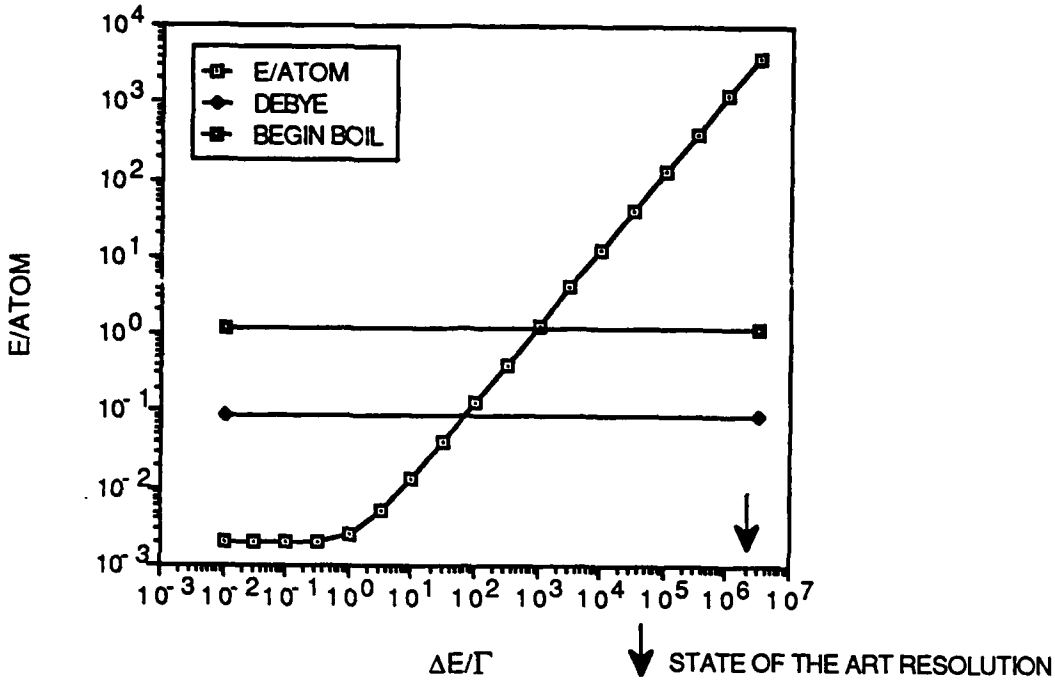

Figure 13. Energy deposition in eV per atom during 1% upconversion of a 0.01 μm ^{57}Fe sample. Current beam resolution is inadequate to prevent severe overheating, even with beams of insufficient intensity.

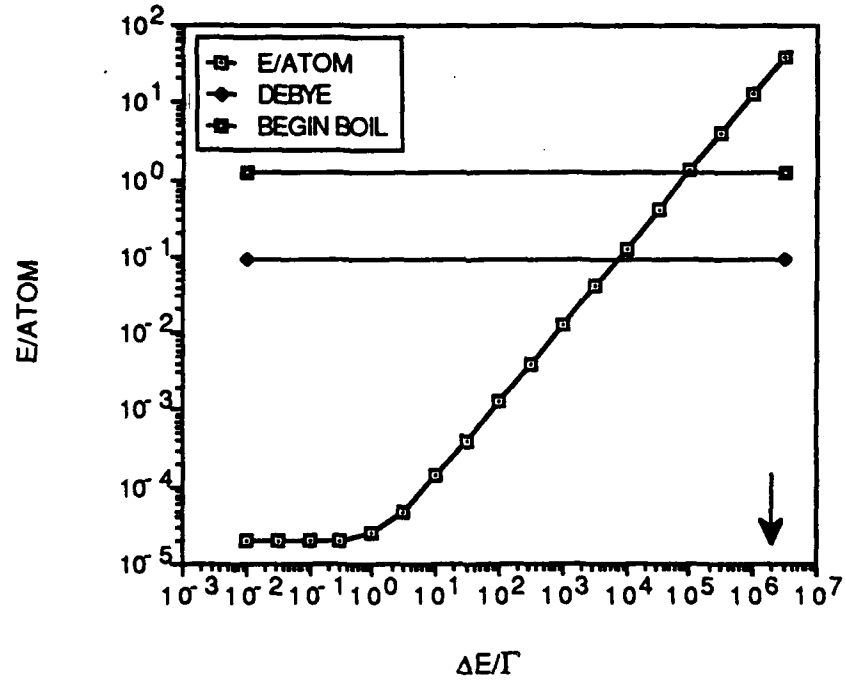

Figure 14. Energy deposition in eV per atom. Same conditions as Fig. 13, but with a factor of 100 reduction in the photoelectric cross section. Overheating is still a problem.

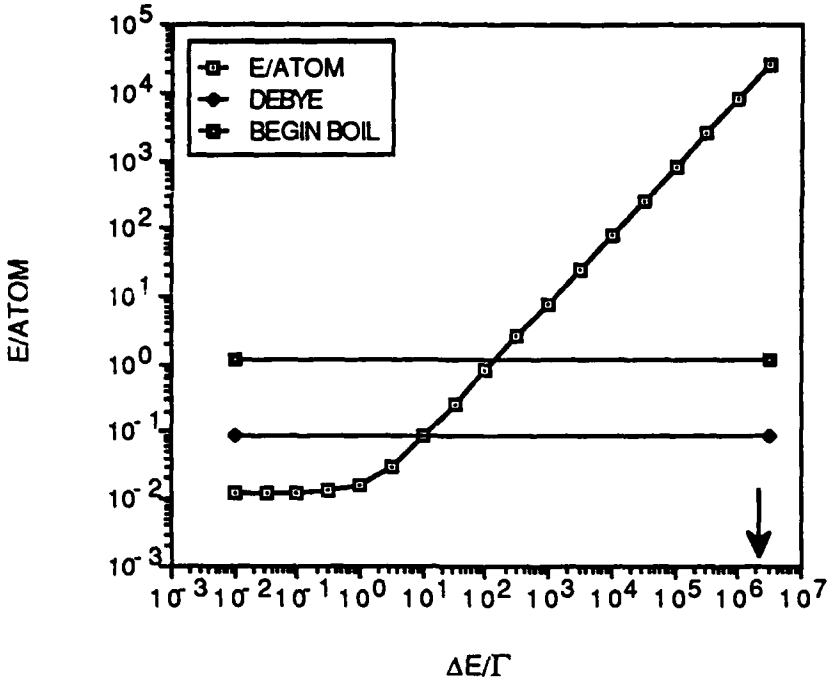

Figure 15. Same as Fig. 14, but for an iron-like target with a 1 keV transition with the same nuclear matrix elements as the 14.4 keV transition. The heating has become much more severe because the photoelectric effect, and the rate at which the photoelectrons deposit energy are both dramatically increased.

natural width of the state already contributes enough energy to heat the sample above the Debye temperature.

This situation will continue to get worse to energies below 100 eV. It may begin to improve at that point because dE/dx of tne photoelectrons begins to decrease. Nevertheless, the heating is probably intolerable for any photons above the minimum ionization threshold.

D. LOOPHOLES

In this section we discuss two proposed loopholes, conductive cooling, and time considerations which might allow triggering of a gamma-ray laser, despite the heating. Conductive cooling of the sample requires that the sample be embedded in or against a material which has a high thermal conductivity, high heat capacity, and low photoelectric cross section. We considered carbon as a candidate heat sink. (Other materials will be considered in the future.) We took the Debye temperature as a target temperature, and computed the energy needed to raise graphite from around 100 K to 440 K, the Debye temperature of iron. Then, for given $\Delta E/\Gamma$ we computed the energy deposited per iron

atom (assuming the Borrmann effect, as in Fig. 14), and converted that to the number of carbon atoms needed per iron atom, and a thickness for the carbon backing. We then computed the direct heating of the carbon backing due to the photoelectric effect in the backing. The carbon was also assumed to be in a crystal with a factor of 100 reduction in the photoelectric cross section due to the Borrmann effect. No account was taken of photoelectrons from one material passing into and heating the other.

Despite these optimistic assumptions, the results shown in Table 6 indicate limited, if any, help from the heat sink. For 0.1 eV resolution beam, we find that the needed carbon heat sink is sufficiently large that despite the lower photoelectric effect, it would be heated above the temperature of the iron, and aggravate the problem. As the postulated beam is improved, the carbon begins to lower the temperature of the iron. Nevertheless, there appears to be no appreciable region where this approach would be helpful. It should be stressed that this again is a conservative calculation, and that substantial heating of the carbon from photoelectrons produced in iron, and vice versa should be expected. On the other hand, berylium or boron, because of their even smaller photoelectric cross sections might be better in this application as heat sinks. Future calculations will address this question.

Table 6. Heatsink temperature (K) due to photoelectric effect in the heatsink itself. Size of heatsink set by excess heating (above T_{DEBYE}) in 0.01 μm Fe sample, initially at 100 K.

$\Delta E/\Gamma$	E_D	T (K)	a (μm)	E_D (C)	T (C)
10^6	23.0		0.32	34.0	Hotter
10^5	2.3	5346	0.1	0.49	Cooler
10^4	0.23	985	0.032	0.0059	320*
10^3	0.023	189	0.01		

*Insufficient for cooling of entire sample below T_{DEBYE}.

Another approach to evading the difficulties presented by heating is to attempt to get the coherent radiation out of the lasing medium before the heat leads to disintegration.

Generally, the lifetimes under consideration are on the order of 10 ns. If they are much shorter, then pump power problems are believed to become insurmountable. The question then is, will the crystal hold together well enough for both the Mössbauer and

Borrmann effects to apply for a time on the order of 10 ns. We believe that this is at present an unanswered question. From the results of Ref. 23 it is clear that the time required for break up of a diffraction pattern is a very strong function of the amount of energy deposited. The data are plotted, along with a simple power law fall-off, in Fig. 16. (The best fit was $t = 6723 \times^{-6.13}$ ps, where x is the energy absorbed divided by the energy required to melt the sample.) This time decreases very rapidly with deposition energy. If barely enough energy is deposited for melting of the sample, the crystal integrity times may be on the order of a few ns in aluminum. If three times the melting energy is deposited, the crystal integrity time extrapolates to a few ps. Since diffraction depends on fixed position, whereas the Mössbauer effect relies on low velocity, the Mössbauer effect would probably be lost on a time scale short compared to that for the diffraction pattern. Characteristic times for electron transit, even at low energy, are quite short compared to the likely lifetimes. (A 100 eV electron travels at 6 μ/ps.) The combination of crystal disintegration times and electron transit times both short compared to the relevant nuclear lifetimes makes lasing before disintegration appear improbable. Further analysis will include electron-photon collision times and atomic excited state photon and auger decay times.

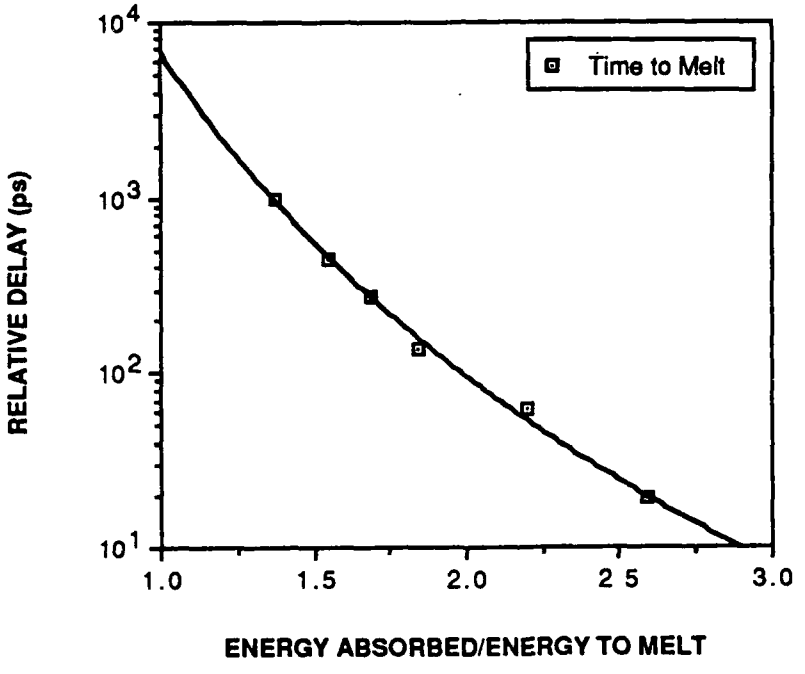

Figure 16. Crystal disintegration times from Ref. 23 as a function of deposited energy. The energy deposition is in units of the energy required to melt the sample.

E. CONCLUSIONS

X-ray upconversion of a nuclear isomer to a suitable lasing state is going to be an extremely difficult undertaking. Intrinsically, leakage of a very small fraction of energy into thermal channels, primarily via the photoelectric effect, will destructively heat the sample. Current X-ray sources are orders of magnitude too broad in energy, as well as too weak to accomplish the task. It appears that the time scales of the destructive heating are short compared to nuclear decay times. A preliminary examination indicates that conductive cooling of the sample is not a workable option. Photoelectric heating of the heatsink itself prevents its utility.

From the above discussion it appears that two courses of action are called for. First, within the context of the upconversion approach to building a gamma-ray laser, much more attention should be paid to possible triggering beams. Furthermore, other approaches not relying on upconversion should be receiving greater attention.

III. AN INVESTIGATION OF THE DESTRUCTION BY INHOMOGENEOUS BROADENING OF RESONANCE IN ISOMERIC CRYSTALS AND ITS RESTORATION BY SPECIAL EFFECTS

A. INTRODUCTION

The first concepts for developing a gamma-ray laser were based on stimulated emission from isomeric crystals (Ref. 24). It was natural to examine the possibility of stimulated emission in long-lived nuclear transitions after (1) the development of the maser and laser showed that inversion was possible and stimulated emission could be used to generate and control coherent microwave and optical radiation (Ref. 6) and (2) the discovery of the Mössbauer effect showed that nuclear resonance fluorescence could be easily observed under well-defined conditions (Ref. 25). The possibility of using nuclear isomeric crystals as the lasing media, the isomeric level being the upper lasing level, was desirable because it would allow the use of lower pumping powers for the inversion.

However, soon after the discovery of the Mössbauer effect, experimental exploration of this phenomenon of nuclear resonance revealed that observing the effect with nuclei of longer lifetimes (narrower natural linewidths) become increasingly more difficult (Ref. 13). The reason for this is that nuclei at different sites in the crystal experienced slightly different electric and magnetic fields because of crystal irregularities, impurities, and even different nuclear spin orientations of nearest neighbors. These effects, collectively referred to as inhomogeneous broadening of the Mössbauer line, will be discussed in more detail later. For the present, it is sufficient to point out that, in order to use isomeric levels in a lasing transition, the inhomogeneous broadening effect on the resonance has to be reduced. Two concepts have been proposed to do just this.

One concept for producing a gamma-ray laser is based on the ability to remove the effect of the coupling which causes inhomogeneously broadened nuclear resonance lines in the isomeric crystal. The technique proposed for eliminating the effects of nuclear dipole-

dipole interaction, a major contributor to the inhomogeneous broadening, is a well-known RF pulsing technique used in high-resolution nuclear magnetic resonance (NMR) spectroscopy (Ref. 26) and theoretically shown to be applicable to Mössbauer spectroscopy (Refs. 27 and 28). Such techniques have been used to reduce the inhomogeneous broadening in NMR work by up to four orders of magnitude (Ref. 29).

In another concept, the individual narrow lines are homogeneously broadened. Overlap of lines and resonance is achieved (Ref. 30) because as a result of this operation all the nuclei in the sample have the same broad lines, which are greater than the inhomogeneous broadening.

Level Mixing Spectroscopy (LEMS) is based on the principle of homogeneous line broadening (Ref. 31). Recently, the application of this technique to a perturbed angular correlation (PAC) type of experiment led to a measurement of a "resonance" in ^{109}Ag.* The effect of this level mixing on a Mössbauer type of experiment has been discussed in recent publications (Refs. 30, and 32). Experiments are being planned to verify these concepts (personal communication, P. Boolchand).

Another way of obtaining homogeneous broadening of resonance lines which leads to greater overlap between source emissions and the absorber cross section is through relaxation phenomena or time-dependent hyperfine interactions (Ref. 33 and 34). These homogeneous broadening effects are well known in the Mössbauer community. Their use in recovering the resonance destroyed by inhomogeneous broadening in the source and absorber experiment has to be investigated.

In this paper we examine the utility of line shifting and broadening techniques to increase the resonance effect in inhomogeneously broadened systems.

B. RESONANT LINESHAPES AND MÖSSBAUER EXPERIMENTS

The interaction between a source and an absorber in a Mössbauer experiment can be described in terms of an emission line and an absorption cross section. If a detector is located as shown in Fig. 17, then for a thin absorber which does not appreciably change the beam line profile, and assuming only resonant absorption,

---

* Strictly speaking this is not a resonance in the Mössbauer sense.

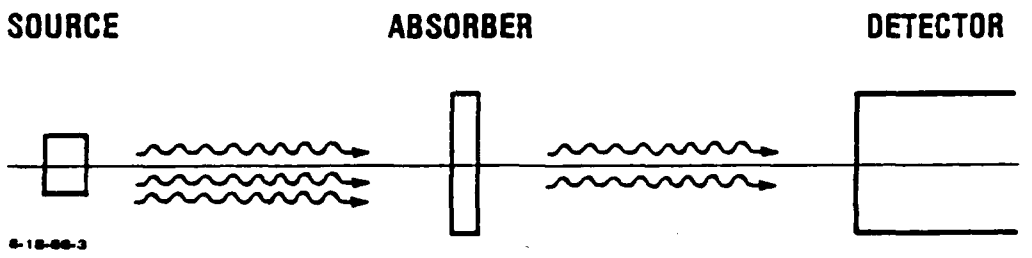

Figure 17. Mössbauer transmission experimental geometry.

the detected loss in the total photon count, I_D, because of the presence of the absorber is given by

$$I_D = \int_{t_1}^{t_2} dt \int_{-\infty}^{+\infty} I(E,\Gamma,S)\, n\, \sigma(E,\Gamma)\, dE \,, \tag{37}$$

where n is the number of resonant nuclei in the beam per cm^2, and the measurement is performed during the time interval $t_2 - t_1$. $I(E,\Gamma,S)$ is the source radiation lineshape and $\sigma(E,\Gamma)$ is the resonant cross section of the nuclei in the absorber.

The source lineshape is given by

$$I(E,\Gamma,S) = \sum_{i}^{N} P_i(\varepsilon_i) \frac{I_0 \left(\frac{\Gamma}{2\pi}\right) f_s}{[E-(E_0-\varepsilon_i) - S]^2 + (\Gamma/2)^2} \,, \tag{38}$$

where I_0 is the flux of photons from the source in $cm^{-2}\, s^{-1}$ in the direction of the detector, E_0 is the resonant energy of an unperturbed nucleus, ε_i is the perturbation of the energy of nucleus i due to the environment, S is the Doppler shift due to the relative motion of the source and absorber nuclei and is given by $S = v/c\, E_0$, with velocity v where c is the speed of light, Γ is the natural linewidth* and f_s is the recoil-free fraction in the source. It is

---

* Γ is the total level width which is a sum of the level widths of all the contributing processes to the level decay.

assumed in equation (37) that the integration time is short enough that I_o can be taken as constant.

The distribution of nuclear environments is assumed to be normal with width Δ so that the probability of finding a nucleus with energy ε_i displaced from the resonance energy E_o in a width $\Delta\varepsilon_i$ is given by

$$P_i(\varepsilon_i) = \frac{1}{\sqrt{\pi}\ \Delta} e^{-\varepsilon_i^2/\Delta^2}\ \Delta\varepsilon_i . \tag{39}$$

Similarly, for the effective cross section of the absorber we have

$$\sigma(E,\Gamma) = \sum_i^N P_i(\varepsilon_i)\ \frac{\sigma_o \Gamma_\gamma \Gamma\ f_a}{[E-(E_o-\varepsilon_i)]^2 + (\frac{\Gamma}{2})^2} . \tag{40}$$

Where σ_o is the cross section on resonance and is given by

$$\sigma_0 = \frac{\lambda^2}{2\pi}\ \frac{2I_e+1}{2I_g+1}\ \frac{1}{1+\alpha} .$$

I_e and I_g are the nuclear spin quantum numbers of the excited and ground states, respectively, α is the internal conversion coefficient of the transition, λ is the nominal wavelength of the gamma-ray, Γ_γ is the photon absorption partial width. Figure 18 is a schematic representation of the resonance effect when ε_i = o. The source and absorber nuclear resonance energies are given by E_s and E_a, respectively, and $\Delta E = E_a - E_s$. The integral over energy given in equation (37) is represented by the shaded region in Fig. 18.

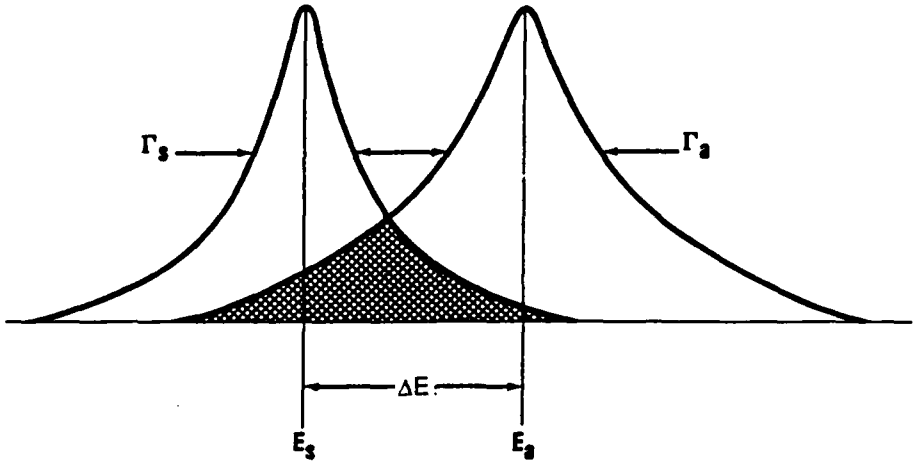

Figure 18. Resonance condition for source and absorber

The usual way of performing Mössbauer experiments is depicted in Fig. 17. One moves the source at predetermined velocities and counts the number of transmitted γ-photons. In this way a Mössbauer transmission spectrum is generated to obtain information about the nuclear electromagnetic interactions.

The Mössbauer effect is defined in (Ref. 35) as

$$\varepsilon(S) = \frac{R\,(S = \infty) - R\,(S)}{R\,(S = \infty)},$$

with the observed counting rate for a "thick" absorber given by

$$R\,(S) = \int_0^\infty I\,(E,\Gamma,S)\,\exp\,[-\mu_t\,(E)\,T]\,dE, \qquad (41)$$

where

$$\mu_t\,(E) = nf\sigma\,(E,\Gamma) + \mu_e\,.$$

In equation (41) μ_e is the linear extinction coefficient which is a function of the photoelectric effect and Compton scattering cross sections, n is the number of resonant nuclei per cm^2, T is the thickness of the absorber in cm, $\beta = fn\sigma_o T$ is usually referred to as the equivalent absorption thickness or the Mössbauer thickness of the absorber (Ref 35).

There are other ways of moving the resonances apart in a controlled fashion than that shown in Fig. 17. One can introduce (1) external DC magnetic fields to shift the resonances; (2) vary the temperature of the samples and thus affect changes in f_a, f_s, and to a much smaller extent, E_o (second-order Doppler shift); or (3) use RF fields to produce zero-order shifts in the energy of the nuclear levels and mix the nuclear states (produce dressed states of nuclei), as suggested by Collins et al. (Ref. 36).

C. INHOMOGENEOUS BROADENING

If the absorber and source were composed of nuclei subjected to the same internal and external fields at the same temperature, the result of the experiment would be essentially as described in equation (37) with $\varepsilon_i = 0$. The signal strength would be a function of the number of nuclei in the path of the beam, ρ_a T A, where ρ_a is the nuclear density in the absorber, T is the thickness of the absorber, and A the area of the absorber illuminated by the beam. This assumes no multiple scattering and a thin sample, so that there is no modification of the beam as it traverses the absorber (effects already well studied by other investigators) (Refs. 35, 37). The actual experimental conditions are generally

quite different. Nuclei imbedded in a solid host interact with the neighboring atoms and change this ideal situation drastically. The effect of impurities, crystal dislocations, and crystal boundaries is to introduce slightly different fields at nuclei located in different positions in the lattice and thereby shift the nuclear resonant energies. The effects are most pronounced for isomeric (long-lived) levels.

Even if the crystal were perfect and we considered only those nuclei well within the regular structure, so that boundary effects were negligible, there would still be a slightly different resonance energy at different lattice sites. The nuclear spin-spin or magnetic dipole-dipole interaction between the emitting or absorbing nuclei and their neighbors would be different due to random orientations of the magnetic moments of different nuclei. This is an inherently nuclear effect and if it were possible to eliminate all the solid state and geometrical factors, this interaction would still remain.

The spin-spin interaction energy is given by

$$E_{d\text{-}d} = \frac{2\,\vec{\mu}_1\,\vec{\mu}_2}{r^3},$$

where μ_1, μ_2 are the magnetic moments of the respective nuclei and r is the distance separating their centers. For ^{107}Ag, this energy has been estimated to be about 10^{-12} eV (Ref. 38). Such a weak interaction is not important in experiments with good Mössbauer nuclei, such as ^{57}Fe, which has a natural linewidth of 5×10^{-9} eV. It has been argued that this interaction essentially destroys resonance between long-lived or isomeric nuclei such as ^{107}Ag or ^{109}Ag because the effective lineshape for the absorber and source is now smeared out over energies much larger than the natural linewidth, which is on the order of 10^{-17} eV.

Inhomogeneous broadening of resonance levels is depicted in Fig. 19, where the resonance condition for a good Mössbauer isotope ^{57}Fe is compared to the resonance condition for a poor Mössbauer isotope, ^{107}Ag.* In view (a) of Fig. 19, the resonances of the emitting and absorbing nuclei are separated by an energy, $\Delta\varepsilon$, which arises because of the slight difference in the local environment of the two nuclei. The natural linewidth, Γ of ^{57}Fe, is large enough that the overlap region provides a good resonance effect. On the other hand, as shown in view (b) of the figure, for the long-lived isotope with the very narrow natural line, the environmental difference between the nuclear sites, which induces

* For the moment, the difference in the recoilless fraction, f, between the two isotopes is ignored.

the energy shift $\Delta\varepsilon$, destroys the resonance condition between emitter and absorber. To properly describe this situation, $\varepsilon_i \neq 0$ has to be introduced into the equations.

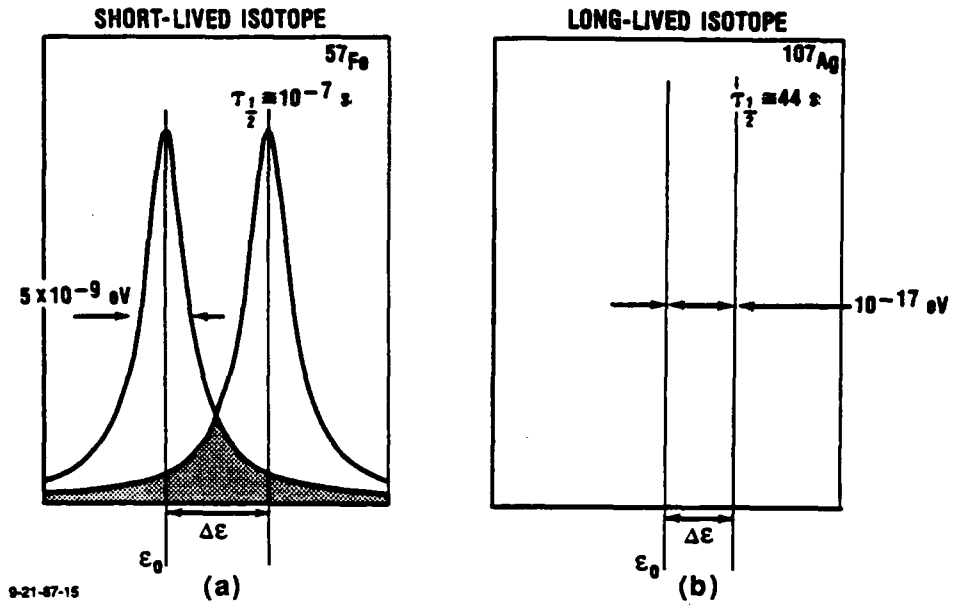

Figure 19. Resonance conditions for short- and long-lived isotopes. For comparison we show in (a) ^{57}Fe a good Mössbauer isotope but difficult to invert because of the short lifetime and in (b) ^{107}Ag, relatively more easy to invert because of the long lifetime but not a good Mössbauer isotope because of the narrow lines.

This parameter can be conveniently divided into three parts so that

$$\varepsilon_i = \varepsilon_{c_i} + \varepsilon_{n_i} + \varepsilon_{e_i}$$

where ε_{c_i} is the energy shift in the resonance of nucleus i due to crystal imperfections, impurities, boundary effects, ε_{n_i} is the energy shift in the resonance of nucleus i due to nuclear spin effects from neighboring nuclei and, ε_{e_i} is due to external effects such as gravitational differences at different nuclei sites.

The average effect on Mössbauer experiments of this inhomogeneous line broadening due to the energy shifts ε_i can be approximated by an effective increase in the linewidth of the source or absorber by a factor (1 + a) where a is called the "inhomogeneous broadening parameter" (Ref. 13). The effect on the threshold condition for lasing is drastic, because the factor (1 + a) multiplies the total linewidth of the nuclei in the lasing medium, thus effectively reducing the resonance cross section.

In the line-narrowing concept for developing a γ-ray laser (Ref. 39), the parameter a has to be substantially reduced. It is assumed that the line-broadening terms due to crystal imperfections and impurities can be reduced by proper geometry, size, and crystal prepartion and that the nuclear spin interaction term can be reduced by an appropriate sequence of RF pulses, as in high-energy resolution NMR. Alternatively, a technique for homogeneously broadening the individual resonance lines such as Level Mixing Spectroscopy (LEMS) can be applied to reduce a. The two mechanisms for achieving resonance in the sample, or more precisely getting more nuclei on resonance are depicted in Fig. 20. In case one the narrow lines are shifted toward E, the unperturbed energy, and in case two the lines are broadened so that the effective linewidth is greater than the energy producing the inhomogeneous broadening. The total magnitude of the required effect is dependent on other isomer characteristics, as discussed in Ref. (39).

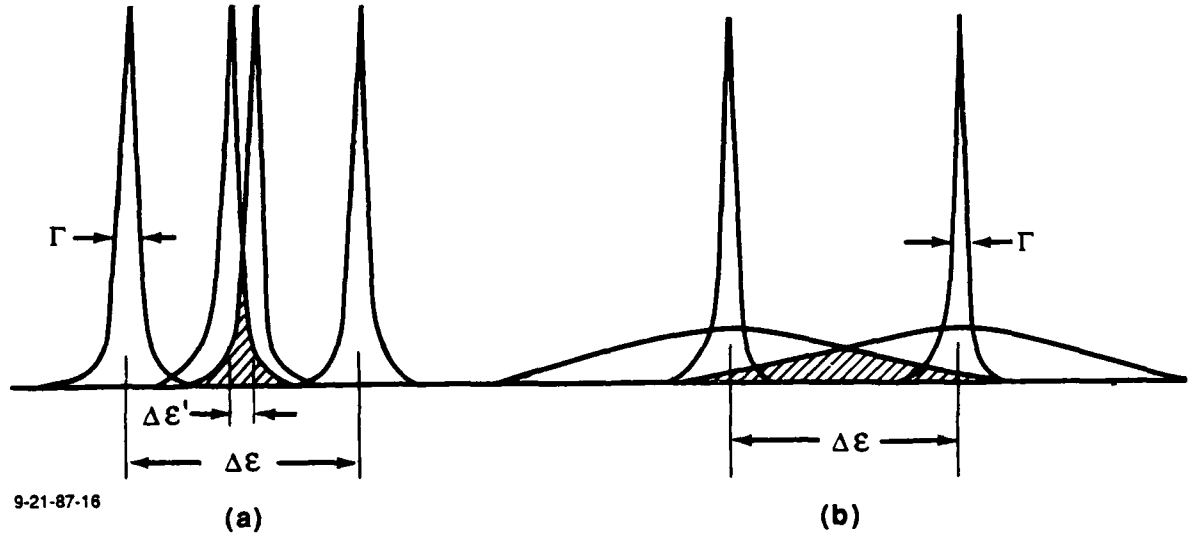

Figure 20. Two different approaches for obtaining resonance with long-lived isotopes (destruction of the effect of inhomogeneous broadening) in (a) an RF pulsing technique causes a line shift and in (b) through cross fields level mixing, or relaxation homogeneous broadening of lines causes resonance overlap.

The inhomogeneous broadening term a will be reduced naturally when either the ground or excited nuclear states have zero spin, because then either μ_1 or μ_2 will be zero. Also, if the nuclei in the crystal are all initially in the excited state the effect of this term will

be greatly diminished in the early stages of laser pulse evolution because of the relatively small number of nuclei in the ground state.

D. THE MÖSSBAUER RESONANCE IN THE PRESENCE OF INHOMOGENEOUS BROADENING

Assuming the source lineshape, absorber cross section, and distribution of nuclear environments as given by equations (38, 39, and 40, respectively) the intensity of the beam I' absorbed by a thin absorber* ($E_0 = 0$ without loss of generality) is given by

$$I'(\Gamma,\Delta,S) = \frac{I_o\sigma_o}{4\pi\Delta_1\Delta_2}\, n_a \sum_i^{N_s} \sum_j^{N_a} e^{-\varepsilon_i^2/\Delta_1^2}\, e^{-\varepsilon_j^2/\Delta_2^2}\, \Delta\varepsilon_i\, \Delta\varepsilon_j$$

$$\times \int_{-\infty}^{+\infty} dE\, \frac{(\Gamma/2\pi)}{(E-\varepsilon_i-S)^2 + (\Gamma/2)^2}\, \frac{\Gamma_\gamma\Gamma}{(E-\varepsilon_j)^2 + (\Gamma/2)^2}\,, \qquad (42)$$

where N_S, N_a are the total number of sites with energy shifts ε_i and ε_j in the source and absorber, respectively, and where n_a is the number of nuclei per cm^2 in the absorber. Converting the sum to an integral one has (see Appendix A)

$$I'(\Gamma,\Delta,S) = \frac{\sqrt{2\pi}}{4}\, I_o\sigma_o(\Gamma_\gamma/\Delta)\, n_a\, \mathrm{Re}\,(e^{Z^2})\, \mathrm{erfc}(Z) \qquad (43)$$

where

$$\Delta^2 \equiv (\Delta_1^2 + \Delta_2^2)/2 \text{ , and } Z \equiv (\Gamma + iS)/\sqrt{2}\,\Delta\,.$$

The maximum normalized resonant absorption ($S = 0$) is given by

$$I''(\Gamma,\Delta) = I'(\Gamma,\Delta,S=0)/\left(\tfrac{1}{2} I_o n_a \sigma_o\right) \qquad (44)$$

$$= \frac{\sqrt{\pi}}{2}\left(\frac{\Gamma_\gamma}{\Gamma}\right)\left[x\, e^{x^2}\, \mathrm{erfc}\, x\right], \quad \text{where } x = \frac{\Gamma}{\sqrt{2}\,\Delta}\,.$$

---

* A thin Mössbauer absorber is one for which the lineshape of the beam passing through the absorber is not sufficiently modified to show saturation effects. This is discussed in Appendix B, where it is shown that for the Mössbauer thickness $b < 10$ the ratios of the intensities of the lines in the spectrum are close to their theoretical values and saturation effects are small. Under such conditions, it is appropriate to use equation (37) for the absorption calculations instead of the general expression given in equation (41).

The definite integrals presented in Appendix C are helpful in examining some special cases of equations (42) and (43). We now examine some special limiting cases assuming $\Delta_1 = \Delta_2$.

Case (a), rare packing. For all i and j in the source and absorber, $\Gamma << |\varepsilon_i - \varepsilon_j|$.

If, in addition to this assumption, the number of nuclei in the sample is small such that, on the average, the near resonance distance is $n\Gamma$, where n is the number of linewidths between resonances as shown in Fig. 20, equation (42) can be reduced to:

$$I' = \frac{I_o \sigma_o n_a}{4\pi\Delta^2}\left(\frac{\Gamma_\gamma}{\Gamma}\right)\int d\varepsilon \int d\varepsilon' \, e^{-\varepsilon^2/\Delta^2} e^{-\varepsilon'^2/\Delta^2} \frac{1}{n^2}$$

$$= \frac{I_o \sigma_o n_a}{2\Delta^2\pi}\left(\frac{\Gamma_\gamma}{\Gamma}\right)\pi\Delta^2 \frac{1}{n^2}$$

$$= \frac{\sigma_o I_o n_a}{2n^2}\frac{\Gamma_\gamma}{\Gamma}.$$

Case b, dense packing with $\Gamma >> |\varepsilon_i - \varepsilon_j|$, for all i.

The linewidth is much greater than the separation between the resonances. This implies that $\Gamma \approx \Delta$. Then,

$$I' = \frac{I_o \sigma_o n_a}{(\pi\Delta)^2}\left(\frac{\Gamma_\gamma}{\Gamma}\right)\int d\varepsilon \, e^{-\varepsilon^2/\Delta^2} \int d\varepsilon' \, e^{-\varepsilon'^2/\Delta^2} \int dx \frac{1}{(x-\varepsilon)^2 + 1}$$

$$= \frac{I_o \sigma_o}{2}\left(\frac{\Gamma_\gamma}{\Gamma}\right) n_a .$$

Case c, dense packing with $\Gamma, S << \Delta$

$$I'(\Gamma,\Delta) = \frac{\sqrt{2\pi}}{4} I_o \sigma_o n_a \frac{\Gamma_\gamma}{\Delta} .$$

Case d, dense packing with Γ or $S >> \Delta$

$$I'(\Gamma,\Delta) \approx \frac{L\, I_o \sigma_o n_a \Gamma_\gamma}{2(\Gamma^2 + S^2)} .$$

The normalized maximum resonance absorption, $I''(\Gamma,\Delta)$ calculated from equation (44) is plotted in Fig. 21 as a function of Γ/Δ for the case $\Gamma/\Gamma_\gamma = 1$, and in Fig. 22 as a function of Δ/Γ for various values of Γ/Γ_γ. For inhomogeneous broadening on the order of the natural linewidth, $\Gamma/\Delta \approx 1$, good absorption is obtained, indicating the presence of a strong Mössbauer resonance between the source and absorber. For $\Delta >> \Gamma$, the absorption drops linearly.

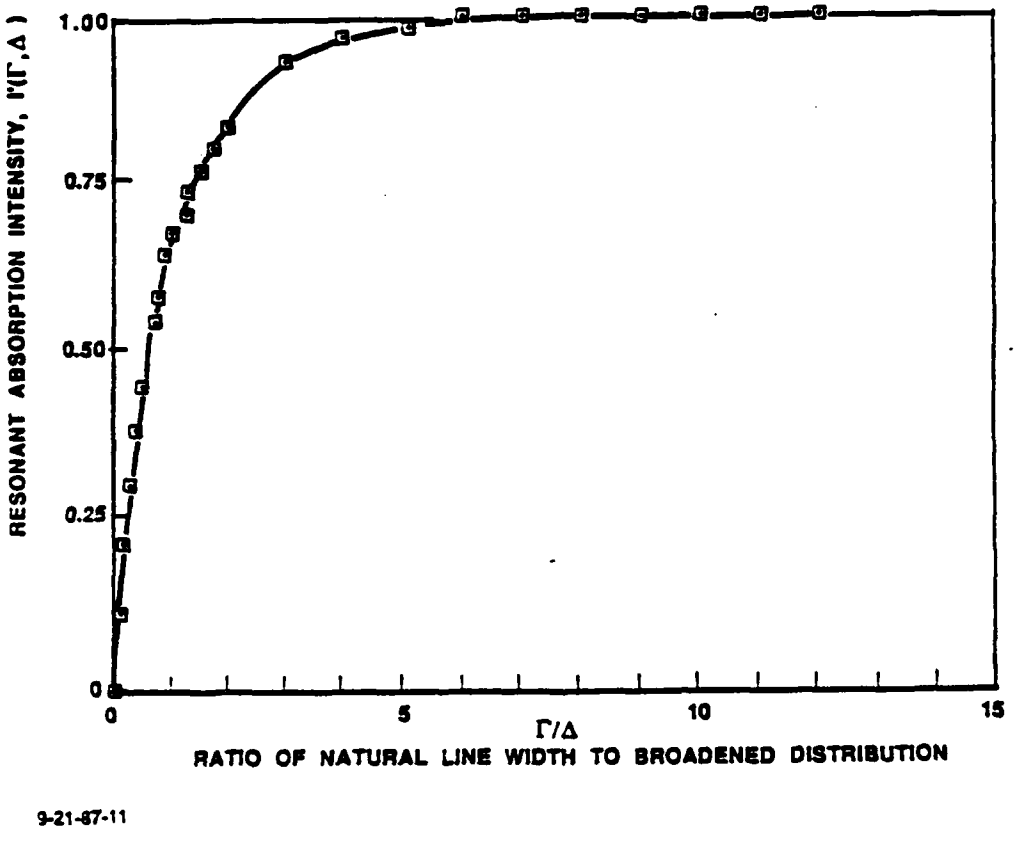

Figure 21. A plot of the maximum normalized resonance absorption I" (calculated from equation (44), assuming $\Gamma_\gamma/\Gamma = 1$) as a function of Γ/Δ .

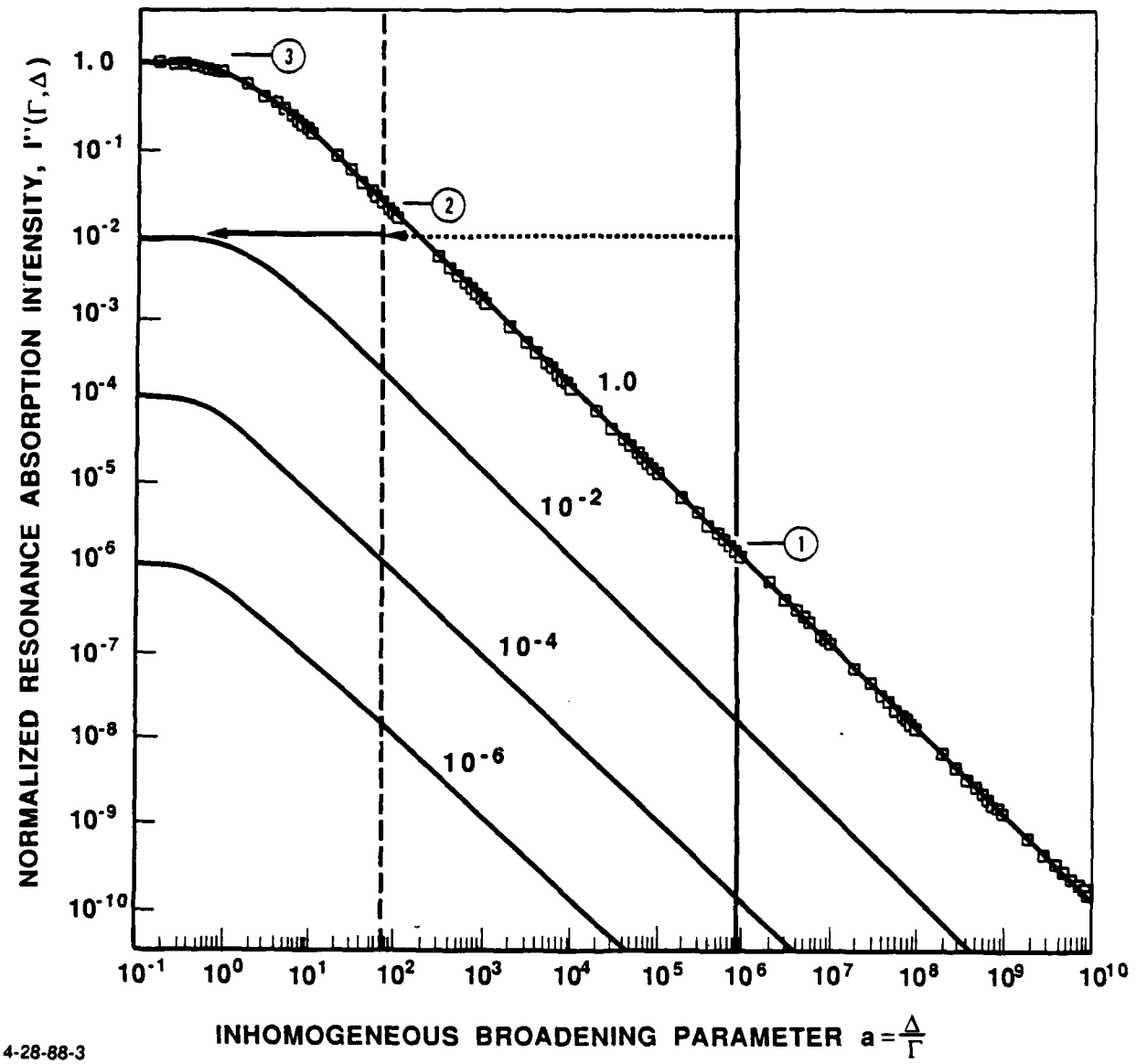

Figure 22. Plots of the maximum normalized resonance absorption curves, $I''(\Gamma,\Delta)$, calculated from equation (44) and plotted as a function of Δ/Γ. The numbers labeling the curves give the different values of Γ_γ/Γ. The dashed horizontal arrow shows the effect on the resonance expected from RF pulsing techniques (Refs. 26 and 29) and the solid arrow the reduction in inhomogeneous broadening expected from good crystal preparation techniques from ordinary isomeric samples with a broadening parameter of a = 10^6.

E. DECREASING THE EFFECT OF INHOMOGENEOUS BROADENING IN MÖSSBAUER EXPERIMENTS

Inhomogeneous broadening results from nuclear environments at different lattice sites producing different shifts in the resonance energies ϵ_i of the respective nuclei. This effect reduces the overlap in the source and absorber lineshapes. In order to increase the overlap, one can either shift the individual resonances back to a common energy E_0, as shown in Fig. 20(a) or broaden the lines homogeneously without shifting, as shown in Fig. 20(b). It may be possible to perform a modification of the lineshape which results in both effects as shown in 20(c). Two approaches to overcome the inhomogeneous broadening effect on Mössbauer experiments have been presented in the literature. Generally, the first step in both techniques is the preparation of a crystal of the isomer, with minimum deformations. However, even in an ideal crystal the dipole-dipole interaction between non-zero spin nuclei will persist and produce different energy shifts at different nuclear positions.

In the first approach, one attempts to reduce the effect of the dipole-dipole interaction by the technique of pulsed RF fields. This technique was originally developed for high-resolution NMR spectrometry and is incorporated into commercial instrumentation (Ref. 26). It has been claimed to reduce inhomogeneous linewidth in nuclear ground state spin transitions by as much as 10^4 (Ref. 29) and has been examined theoretically as a procedure for reducing the inhomogeneous broadening in Mössbauer effect experiments (Ref. 27). It reduces the inhomogeneous linewidth by breaking the effect of the dipole-dipole interaction through rapid reorientation of the spins, thus effectively shifting lines toward the same resonance energy $\Delta\epsilon \rightarrow \Delta\epsilon' \rightarrow 0$ for all i) as shown in Fig. 20(a). With reference to Fig. 22, the resulting decrease in Δ would move the operating point from point (1) to point (2) on the curve, reflecting a decrease in Δ/Γ of 10^4. To approach the desired operating point (3) a further reduction in Δ would have to be achieved by proper preparation for the crystal to minimize the effect of impurities and crystal imperfections.

The second technique is depicted in Fig. 20(b). Instead of shifting the resonance energy at each nucleus by $-\epsilon_i$ to coincide with the base nuclear resonant energy [see equation (42)] the second technique homogeneously broadens each line to obtain greater overlap in the lineshapes as shown in Fig. 20(b). The homogeneous line broadening can be achieved by various means. In particular by working in the region of level crossings,

mixing of sublevels can provide enhanced transitions between sublevels leading to homogeneous broadening of lines.

The reduction of the overlap of nuclear resonance lines in an inhomogeneously broadened crystal is depicted in Fig. 23(a). Only some of the lines are shown for clarity presentation. Partial recovery of the overlap due to line shifts, homogenous broadening, and a combination of the two effects is depicted in Fig. 23(b) through 23(g).

Level mixing effects have been used in Level Mixing Spectroscopy (LEMS) to obtain resonances in perturbed angular correlation experiments in ^{109}Ag (Ref. 31). Such resonances have not been seen before in the Ag transition and are not seen outside of the level crossing region, indicating the importance of the shortened coherence time in these experiments. In Mössbauer experiments, on the other hand, the value of the resonance cross section determines the size of the effects. If this broadening is done at the expense of the maximum cross section on resonance, then as can be seen from equations (40) and (43) an increase in the total width Γ will not be effective in producing an increase in resonance as $\Gamma \rightarrow \Delta$ because the factor Γ_γ/Γ in equation (44) will still dominate even though Γ/Δ the argument in the exponential and error function factors increases to values greater than one . The homogeneous broadening produces overlap of lines but this is not sufficient to get good absorption because of the factor Γ_γ/Γ. The mechanism (LEMS) has to induce level shifts in addition to homogeneous broadening in order to be effective.

Another way of obtaining homogeneous broadening is through relaxation effects which are clearly exhibited in Mössbauer effect spectra. Figure 24 shows Mössbauer transmission spectra of Ferrichrome A, a paramagnetic compound, at several temperatures. The spectra range from a well-defined, six-line pattern with narrow lines approaching the natural linewidth at low temperatures to a complex broadened pattern with linewidths determined by the electron spin relaxation time and the magnitude of the interaction to a single motionally narrowed peak, with the hyperfine pattern destroyed at high temperatures.

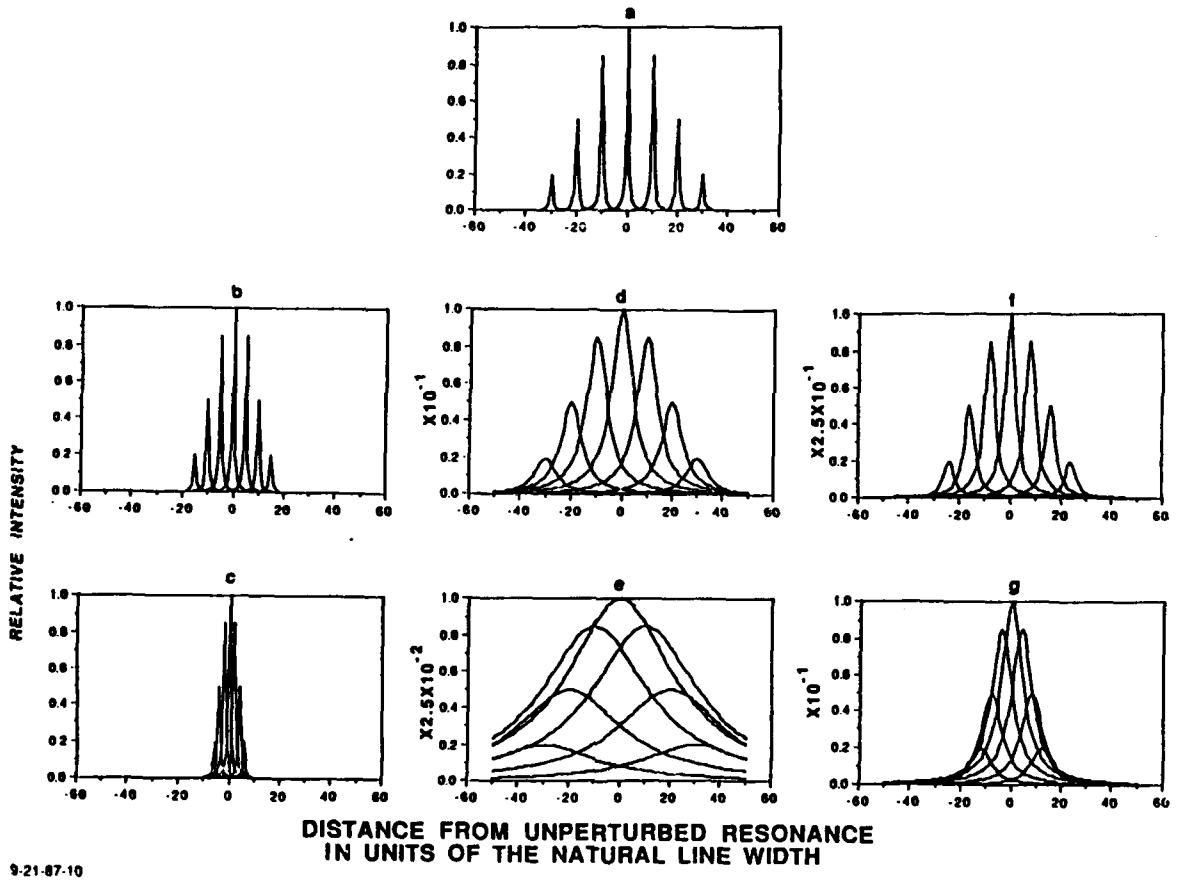

Figure 23. Reduction of the overlap of nuclear lineshapes in an inhomogeneous crystal (a) and partial recovery of the overlap due to line shifts (b, c) homogeneous broadening (d, e) and a combination of the two (f, g). Note the decrease in the relative intensities as the width increases (d,e,f,g).

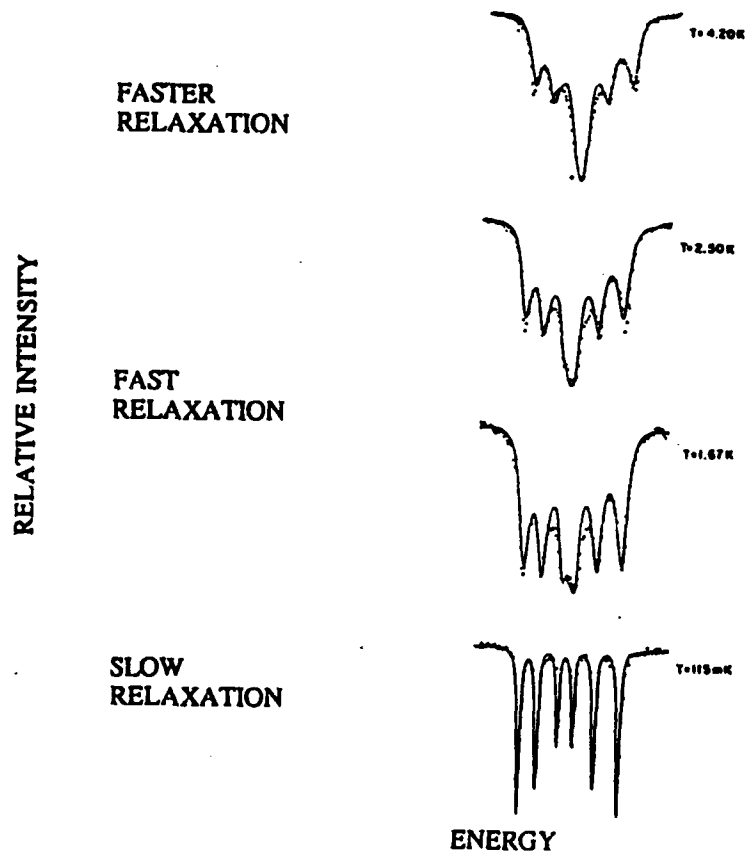

Figure 24. Nuclear lineshape modification due to electronic relaxation without change in the nuclear lifetime: experimental results in Ferrichrome A are shown, together with the theoretical calculation. Source of data is Ref. 34.

Figure 25 shows a hypothetical source absorber overlap of lines with narrow lines in Fig. 25(a) and broadened lines in Fig. 25(b), and 25(c). For the case depicted in Fig. 25(a) the Mössbauer effect, which is dependent on the overlap integral, is proportional to $\Gamma_\gamma\Gamma/\Delta E^2$, whereas in cases (b) and (c) it is proportioned to $(\Gamma_\gamma/\Delta E)$; an increase by a factor of $\Delta E/\Gamma$.

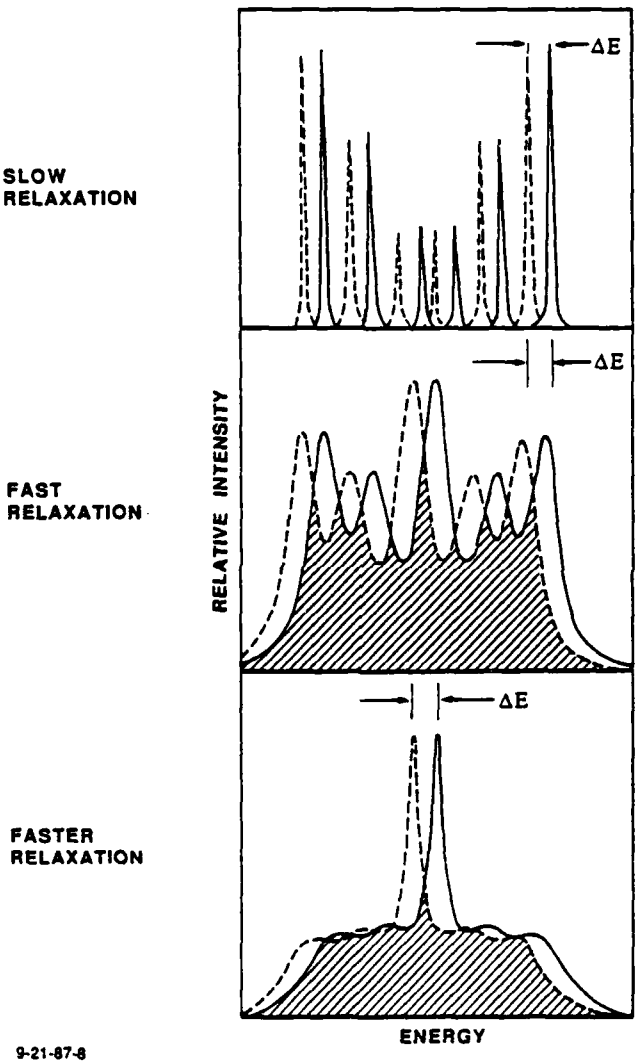

Figure 25. Nuclear lineshape modification due to electronic relaxation without change in the nuclear lifetime for two different relaxation roles. The solid and dashed curves represent the source and absorber lineshapes, respectively. The shaded region indicates the overlap.

F. CONCLUSIONS

In a source-absorber experiment where both the source and absorber are inhomogeneously broadened and the distribution of fields at the individual nuclear sites is normal, the Mössbauer effect is inversely proportional to the width of the distribution. The resonance effect can be restored, in general, by removing the energy shifts at the individual sites but not simply by homogeneously broadening the lines, even though significant overlap is achieved. Under special conditions, homogeneous broadening of lines will provide an increase in the Mössbauer effect. Such special conditions can occur if the broadening is accompanied by a significant lineshift toward the mean of the line positions or if the broadening produces an interaction between nuclei, leading to cooperative effects and a speed up of the radiative decay, as in Dicke superradiance.

REFERENCES

1. B. Balko, L. Cohen, and F.X. Hartmann, Eds., *IDA Gamma-Ray Laser Annual Summary Report (1985): Investigation of the Feasibility of Developing a Laser Using Nuclear Transitions*, IDA Paper P-2021, June 1986.

2. B. Balko, L. Cohen, and D. Sparrow, *IDA Gamma-Ray Laser Annual Summary Report (1986): Investigation of the Feasibility of Developing a Laser Using Nuclear Transitions*, IDA Paper P-2004, December 1988.

3. D.J. Nagle, *Phys. Fenn.*, **9**, 381, Suppl. 1, 1974.

4. J.M. Blatt and V.F. Weisskopf, *Theoretical Nuclear Physics*, John Wiley & Sons, New York, 1952.

5. M.G. Mayer and J.H.D. Jensen, *Elementary Theory of Nuclear Shell Structure*, John Wiley & Sons, New York, 1955.

6. H.A. Bethe, *Rev. Mod. Phys.*, **9**, 69, 1937.

7. W.E. Lamb, *Phys. Rev.*, **55**, 190, 1939.

8. A.L. Schawlow and C.H. Townes, *Phys. Rev.*, **112**, 1940, 1958.

9. R.W. Hansch and A.L. Schawlow, *Opt. Commun.*, **13** (1), 68, 1975.

10. W.D. Phillips et al., NBS Special Publication 653, 1, 1983.

11. W. Ertmer et al., *Phys. Rev. Lett.*, **54**, 996, 1985.

12. W.D. Phillips, private communication.

13. R. Bassel, J. Kidd, and N. Seeman, Naval Research Laboratory and S. Penner, National Bureau of Standards, private communications.

14. A. Artna-Cohen, "Compilation of Low-energy Gamma Rays," *J. Quant. Spectrosc. Radiat. Transfer (JQSRT)*, **40** (6), 663, December 1988.

15. G.C. Baldwin, J.C. Solem, and V.I. Gol'danskii, *Rev. Mod. Phys.*, **53**, 687, 1981.

16. C. Collins, F.W. Lee, D.M. Shemwell, and B.D. DePaola, *J. Appl. Phys.*, **53** (7), 4645, 1982.

17. G.C. Baldwin, *Bull. Am. Phys. Soc.*, **32**, 1060, 1987.

18. G.C. Baldwin, private communication.

19. A.H. Muir, K.J. Ando, and H.M. Coogan, *Mössbauer Effect Data Index 1958-1965*, Wiley, 1966.

20. C.G. Wolh et al., *Rev. Mod. Phys.*, **56**, No. 2, Part II, S57, 1984.

21. M.J. Berger and S.M. Seltzer, "Stopping Powers and Ranges of Electrons and Positrons," NBSIR 82-2550-A, 1983.

22. G. Faigel et al., *Phys. Rev. Lett.*, **58**, 2699, 1987.

23. S. Williamson, G. Mourou, and J.C.M. Li, *Phys. Rev. Lett.*, **52**, 2364, 1984.

24. V. Vali and W. Vali, *Proc. IEEE*, **51**, 182 and 1248, 1963.

25. R.L. Mössbauer, *Z. Phys.*, **151**, 124, 1958.

26. M. Mehring, *Principles of High Resolution NMR*, Springer-Verlag, Berlin, Heidelberg, New York, 1983.

27. A.V. Andreev, Y.A. Il'inskii, and R.V. Khokhlov, *Sov. Phys. - JETP*, **40**, 819, 1975.

28. Y.A. Il'inskii and R.V. Khokhlov, *Sov. Phys. - JETP*, **38**, 809, 1974.

29. W.K. Rhim, personal communication.

30. R. Coussement, P. Boolchand, G. Scheveneels, F. Hardemann, and P. Put, *J. Quant. Spectrosc. Radiat. Transfer (JQSRT)*, **40** (6), 773, December 1988.

31. R. Coussement, P. Put, G. Sheveneels, F. Hardeman, *Hyperfine Interact.*, **23**, 273, 1985.

32. R. Coussement, F. Hardeman, P. Boolchand, International Conference on Mössbauer Applications, Australia, 1987.

33. M. Blume in *Hyperfine Structure and Nuclear Radiations*, edited by Mathias and Shirley, North Holland Publishing Co.

34. G.R. Roy, M. Corson, B. Balko, *Phys. Rev. B.*, **27** (5), 2652, 1983.

35. S.L. Ruby and J.M. Hicks, *Rev. Sci. Instrum.*, **33**, 27, 1962.

36. C.B. Collins, F.W. Lee, D.M. Shemwell, and B.D. DePaola, *J. Appl. Phys.*, **53** (7), 4645, 1982.

37. B. Balko, G.R. Hoy, *Phys. Rev. B*, **10**, 4523, 1974.

38. G.E. Bezina, A.G. Beda, N.A. Burgor, A.B. Davidov, *Sov. Phys. JETP*, **18**, 973, 1964.

39. B. Balko, W. Wasylkiwskyj in "*Proceedings of the IST/IDA Gamma-Ray Laser Workshop*," Eds, B. Balko, L. Cohen, F.X. Hartmann, IDA Memorandum Report M-162, January 1986.

APPENDIX A

EVALUATION OF THE THIN ABSORBER INTENSITY

APPENDIX A

EVALUATION OF THE THIN ABSORBER INTENSITY

In Section III-D, the intensity of a beam, I', transmitted by a thin absorber was considered; the results were used primarily for the special case of S=0, that is, coincident distributions of lines in the source and absorber. In this appendix, the details of the derivation of the beam intensity are given for all S and for absorber and source line distributions of different widths. In integral form, the intensity for unit density ($n_a = 1$) is given by

$$I' = \frac{I_0\sigma_0\Gamma^2\Gamma_\gamma}{2\pi^2\Delta_1\Delta_2}\int_{-\infty}^{+\infty}\int\int d\varepsilon_1\, d\varepsilon_2\, dE\, \frac{e^{-\varepsilon_1^2/\Delta_1^2}}{(E-S-\varepsilon_1)^2+(\Gamma/2)^2}\,\frac{e^{-\varepsilon_2^2/\Delta_2^2}}{(E-\varepsilon_2)^2+(\Gamma/2)^2}, \qquad (A.1)$$

where Δ_2 and Δ_2 are the source and absorber widths, respectively. The integral over E is easily performed by contour integration.

$$I' = \frac{2I_0\sigma_0\Gamma_\gamma\Gamma}{\pi\Delta_1\Delta_2}\int_{-\infty}^{+\infty}\int d\varepsilon_1\, d\varepsilon_2\, \frac{e^{-\varepsilon_1^2/\Delta_1^2-\varepsilon_2^2/\Delta_2^2}}{(\varepsilon_2-\varepsilon_1-S)^2+\Gamma^2}\,. \qquad (A.2)$$

The remaining integrations are simplified by a change of variables to:

$$y = \varepsilon_2 - \varepsilon_1$$

$$x = \frac{\varepsilon_1\Delta_2^2}{\Delta_1^2+\Delta_2^2} + \frac{\varepsilon_2\Delta_1^2}{\Delta_1^2+\Delta_2^2}\,. \qquad (A.3)$$

In these variables, the x and y integrals can be done independently.

$$I' = \frac{2I_0\sigma_0\Gamma_\gamma\Gamma}{\pi\Delta_1\Delta_2}\int_{-\infty}^{+\infty}\int dx dy\, \frac{e^{-2\Delta^2x^2/\Delta_1^2\Delta_2^2}\,e^{-y^2/2\Delta^2}}{(y-S)^2+\Gamma^2}\,, \qquad (A.4)$$

where $2\Delta^2 = \Delta_1^2 + \Delta_2^2$. The integral over x is trivial, leaving the following integral for the intensity:

$$I' = \sqrt{\frac{2}{\pi}} \frac{I_0 \sigma_0 \Gamma_\gamma \Gamma}{\Delta} \int_{-\infty}^{+\infty} dy \frac{e^{-y^2/2\Delta^2}}{(y-S)^2 + \Gamma^2} \quad . \tag{A.5}$$

This final integral is performed by rewriting the denominator via a Laplace transform:

$$I' = \sqrt{\frac{2}{\pi}} \frac{I_0 \sigma_0 \Gamma_\gamma}{\Delta} \mathrm{Re} \int_{-\infty}^{+\infty} dy \int_0^{+\infty} ds\, e^{-y^2/2\Delta^2 - s[\Gamma - i(y-S)]} \quad , \tag{A.6}$$

where Re denotes the real part of the integral. The integration over y is now trivial and the final answer is given in terms of the integral over s which is easily recognized as the complementary error function. Thus, the intensity of the beam is given by:

$$I' = \sqrt{2\pi} \frac{I_0 \sigma_0 \Gamma_\gamma}{\Delta} \mathrm{Re}\, e^{z^2} \mathrm{erfc}(z)$$

$$z = \frac{\Gamma + iS}{\sqrt{2}\Delta} \quad . \tag{A.7}$$

This exact combination of exponential and error function is tabulated in standard references (for example, "*Handbook of Mathematical Functions*", edited by Abramowitz and Stegun; note that in this reference z is replaced by -iz, effectively interchanging the real and imaginary parts).

The expression given above can be confirmed in several limits. For $\Delta \Rightarrow 0$ (Γ and/or $S \Rightarrow \infty$), the gaussians in ε_1 and ε_2 in the original form of the integral can be replaced with delta functions giving the simple expression

$$I' = \frac{2 I_0 \sigma_0 \Gamma_\gamma \Gamma}{S^2 + \Gamma^2} \quad , \tag{A.8}$$

which is also obtained from the above expression if it is noted that for large z

$$e^{z^2} \mathrm{erfc}\,(z) \approx \frac{1}{\sqrt{\pi}\, z} \tag{A.9}$$

and taking the real part. On the other hand, for $\Delta \Rightarrow \infty$ (Γ and $S \Rightarrow 0$), the exponential in the final integral over y can be neglected, yielding

$$I' = \sqrt{2\pi}\,\frac{I_0\sigma_0\Gamma_\gamma}{\Delta}\ , \qquad \text{(A.10)}$$

in agreement with the above expression for z = 0.

REFERENCE, APPENDIX A

A-1. M. Abramowitz and I. Stegun, Eds., *Handbook of Mathematical Functions*, Dover Publishing, New York, 1972.

APPENDIX B

A DISCUSSION OF THE EFFECTS ON LINESHAPE OF THE MÖSSBAUER THICKNESS PARAMETER

APPENDIX B

A DISCUSSION OF THE EFFECTS ON LINESHAPE OF THE MÖSSBAUER THICKNESS PARAMETER

The Mössbauer thickness parameter is defined as $\beta = n\sigma_0 fT$ where n is the number of nuclei per cm^3 in the beam, σ_0 is the maximum resonant cross sections, f is the recoilless fraction, and T is the thickness of the sample. The Mössbauer spectrum for large β is affected by the thickness in a complex way due to saturation effects but generally for $\beta < 10$ such effects are unimportant. Figure B-1(a) shows a Mössbauer scattering spectrum obtained from an iron bar with a natural content of ^{57}Fe ($\approx$2 percent). The ratio of line intensities approaches the 3:2:1 ratio expected theoretically for small β. In Fig. B-1(b), for comparison, the results for a sample enriched in ^{57}Fe is shown. The saturation effects are clearly evident when comparison is made with the expected line intensities shown in Fig. B-2. In both Figs. B-1(a) and B-1(b) the solid curves represent calculated spectra for the respective cases (Ref. B-1).

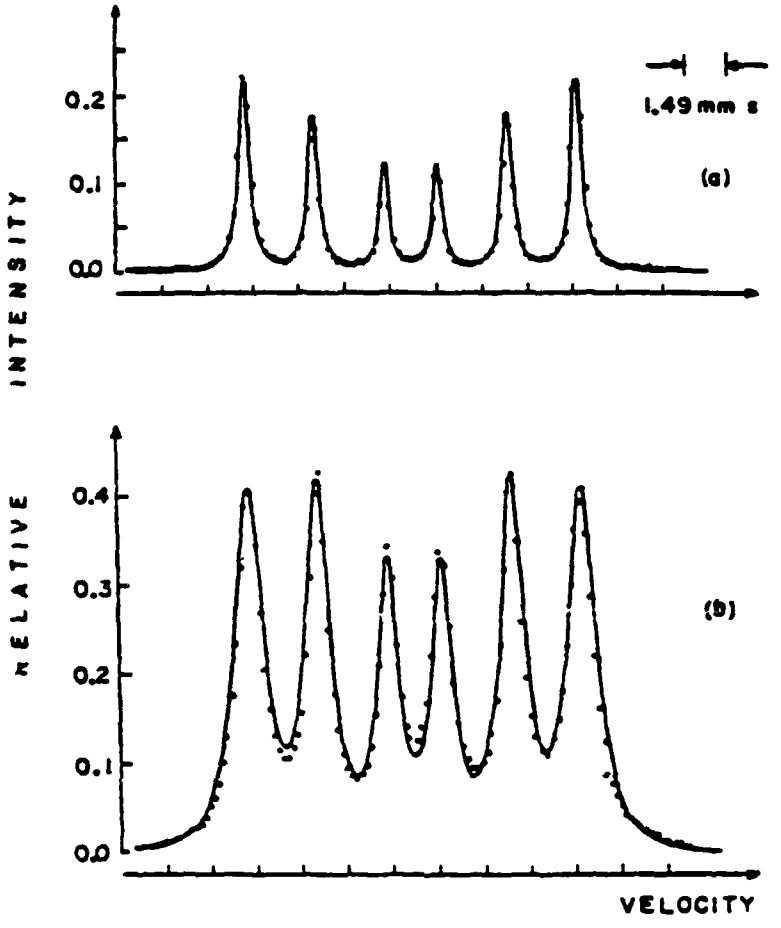

FIGURE B-1. (a) Experimental and theoretical scattering results for a 1/8-in.-thick iron bar at room temperature having the natural content of ^{57}Fe (2%). The dots are the data and the solid curve is the calculated result. The only free parameter is the percent effect at one peak. (b) Same kind of results as shown above but the scatterer is a 90% enriched iron powder (f = 0.8 and β = 175) at room temperature (Ref. B-1).

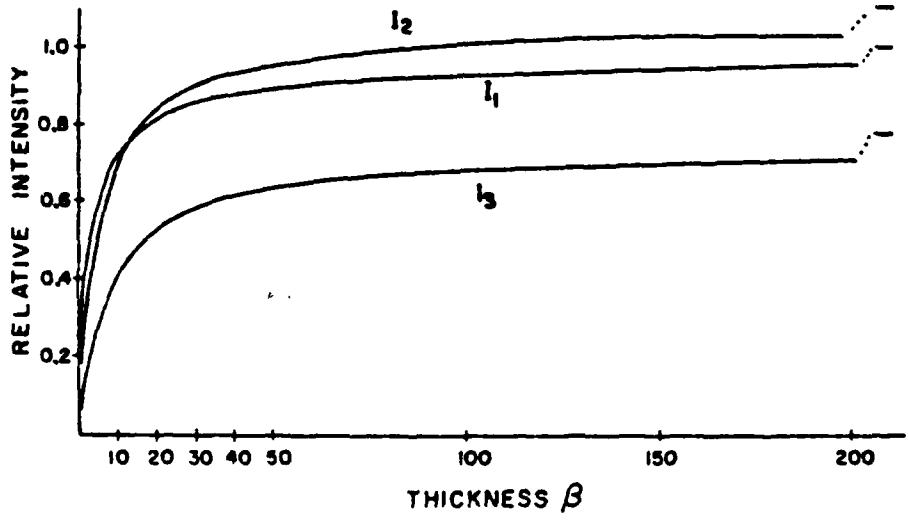

FIGURE B-2. Calculated saturation effect is shown for iron-powder scattering results. The curves are normalized so that $I_1 = 1$ at $\beta = \infty$ (Ref. B-1).

REFERENCE, APPENDIX B

B-1. B. Balko, G.R. Hoy, *Phys. Rev. B*, **10**, 4523, 1974.

APPENDIX C

SOME DEFINITE INTEGRALS USEFUL IN LINESHAPE EVALUATION

APPENDIX C

SOME DEFINITE INTEGRALS USEFUL IN LINESHAPE EVALUATION

DEFINITE INTEGRALS

$$\int_{-\infty}^{+\infty} \frac{dx}{\left(1+x^2\right)\left[1+\left(x-x_o\right)^2\right]} = \frac{2\pi}{x_o^2+4} \tag{C.1}$$

$$\int_{0}^{\infty} e^{-a^2x^2}\, dx = \frac{1}{a}\sqrt{\pi} \tag{C.2}$$

$$\int_{-\infty}^{+\infty} \frac{dx}{1+x^2} = \pi \tag{C.3}$$

$$\int_{-\infty}^{\infty} \frac{dx}{\left(1+x^2\right)^2} = \pi/2 \tag{C.4}$$

$$\int_{0}^{x} \frac{dx}{a^2+x^2} = \frac{1}{a}\tan^{-1}\left(\frac{x}{a}\right) \tag{C.5}$$

$$\int_{-\infty}^{+\infty} dx dx' \, e^{-\left(x^2 + x'^2\right)/\Delta^2} \left(\frac{1}{\left(x - x'\right)^2 + \Gamma^2} \right) \qquad \text{(C.6)}$$

$$= \frac{\pi}{\eta} \sqrt{\frac{\pi}{2}} \, e^{\eta^2/2} \operatorname{erfc}\left(\eta / \sqrt{2}\right) \text{ where } \eta = \frac{\Gamma}{\Delta}$$

EVALUATION OF INTEGRAL

$$\frac{1}{\left(1+x^2\right)\left[1+\left(x-x_o\right)^2\right]} = \frac{Ax+B}{1+x^2} + \frac{Cx+D}{1+\left(x-x_o\right)^2}$$

$$A = \frac{2}{x_o\left(x_o^2+4\right)},\ B = \frac{1}{x_o^2+4},\ C = \frac{-2}{x_o\left(x_o^2+4\right)},$$

$$D = \frac{3}{x_o^2+4}.$$

$$I = \int_{-\infty}^{+\infty} \frac{dx}{\left(1+x^2\right)\left[1+\left(x-x_0\right)^2\right]} = A\int \frac{x}{1+x^2}\,dx + B\int \frac{dx}{1+x^2}$$

$$C\int \frac{x}{1+\left(x-x_0\right)^2}\,dx + D\int \frac{dx}{1+\left(x-x_0\right)^2}$$

$$\int_{-\infty}^{+\infty} \frac{dx}{1 + \left(x - x_0\right)^2} \Rightarrow \int \frac{dy}{1 + y^2} = \tan^{-1} y \Big]_{-\infty}^{+\infty} = \tan^{-1}\left(x - x_0\right) \Big]_{-\infty}^{+\infty} = \pi$$

$$I = B\pi + D\pi + C\pi = \frac{\pi}{x_0^2 + 4} + \frac{3\pi}{x_0^2 + 4} - \frac{2\pi}{x_0^2 + 4} = \frac{2\pi}{x_0^2 + 4}$$